

Probing double-aligned two Higgs doublet models at LHC

Shinya Kanemura,^{*} Michihisa Takeuchi,[†] and Kei Yagyu[‡]

Department of Physics, Osaka University, Toyonaka, Osaka 560-0043, Japan

Abstract

We consider two Higgs doublet models (THDMs) with both the Higgs potential and Yukawa interactions being aligned, which we call “double-aligned THDMs”. In this scenario, coupling constants of the discovered Higgs boson to the Standard Model (SM) particles are identical to those of the SM Higgs boson, and flavor changing neutral currents via neutral Higgs bosons do not appear at tree level. We investigate current constraints and future prospects of the model by using measurements from flavor experiments and data of multi-lepton final states at LHC. Especially, we focus on the electroweak pair production of the additional Higgs bosons with their masses below $2m_t$. We find that the most of the parameter space are already excluded by the current LHC data when the leptonic decays of the additional Higgs bosons are dominant, which can be interpreted to the scenario in the Type-X THDM as a special case. We also clarify the parameter region where the high-luminosity LHC can explore, and demonstrate the reconstruction of the masses of additional Higgs bosons from the $b\bar{b}\tau^+\tau^-$ final states in a few benchmark points.

arXiv:2112.13679v1 [hep-ph] 27 Dec 2021

^{*} kanemu@het.phys.sci.osaka-u.ac.jp

[†] m.takuechi@het.phys.sci.osaka-u.ac.jp

[‡] yagyu@het.phys.sci.osaka-u.ac.jp

I. INTRODUCTION

The nature of the electroweak (EW) symmetry breaking is one of the biggest mysteries in the elementary particle physics even after the discovery of the Higgs boson at LHC. Although the Higgs mechanism in the standard model (SM) can parameterize the EW symmetry breaking and can explain currently measured properties of the Higgs boson, the true structure of the Higgs sector is still unknown as it is not determined by a fundamental principle. In fact, various possibilities of non-minimal structures of the Higgs sector can be considered without any contradiction with the current experimental data. Therefore, comprehensive studies of extended Higgs sectors are important to understand the nature of EW symmetry breaking as a bottom-up approach.

Two Higgs doublet models (THDMs) are one of the simplest examples of the extended Higgs sector, which naturally satisfy the electroweak rho parameter to be unity at tree level. In addition, THDMs are well motivated, because they appear in various new physics scenarios such as supersymmetry [1], a neutrino-philic model [2], models with radiative generations of neutrino masses [3–5], those with dark matter [6], those with new sources of CP violation (CPV) and those with strongly first order EW phase transitions [7–9]. In particular, such CPV and first order EW phase transitions can be used in the successful scenarios of the electroweak baryogenesis [8–13]. Thus, among the many possibilities of non-minimal Higgs sectors, THDMs should phenomenologically be examined with a special attention.

It has been well known that THDMs generally give rise to flavor changing neutral currents (FCNCs) via neutral Higgs boson exchanges at tree level. In order to avoid such FCNCs, a natural flavor conservation scenario [14] has often been considered, where only one of the Higgs doublets couples to each type of charged fermions, i.e., up-type quarks, down-type quarks and charged leptons. This scenario can naturally be realized by introducing a discrete Z_2 symmetry to the Higgs sector, in which four independent type of Yukawa interactions appear [15–17], the so-called Type-I, Type-II, Type-X and Type-Y. As an alternative possibility to avoid tree level FCNCs, the Yukawa alignment scenario has also been discussed [18], in which two Yukawa matrices for each type of charged fermions are assumed to be proportional with each other. In this case, Yukawa couplings can generally be complex, so that we can consider two independent CPV sources in the Yukawa interactions and the Higgs potential.

Apart from the Yukawa alignment, current LHC data show that measured properties of the discovered Higgs boson agree with those of the SM Higgs boson within the uncertainty. This suggests that one of the neutral Higgs bosons in the THDM, denoting h , must have SM-Higgs

like properties. There are two ways to realize such a situation, i.e., taking decoupling or alignment regions of the parameter space. The former corresponds to the case with all the masses of additional Higgs bosons being much higher than the EW scale, in which properties of h approach to those of the SM Higgs boson according to the decoupling theorem [19, 20]. On the other hand, the latter can be realized by taking the h state being aligned to be one of the states in the Higgs doublet which possesses the vacuum expectation value (VEV) same as in the SM ¹. Unlike the decoupling case, the scenario with the “Higgs alignment” provides phenomenologically interesting consequences, because the additional Higgs bosons can be at the EW scale, which is often referred as “alignment without decoupling” [22]. ² From the above mentioned reasons, THDMs with the Yukawa and Higgs alignment provide a phenomenologically interesting scenario. We call this type of scenario as “double-alignment”. Recently in Ref. [43], such a double-aligned scenario has been studied, and found that sizable CPV phases can be taken without contradiction to bounds from current data of electric dipole moments (EDMs) [44, 45] as well as flavor experiments and LHC experiments. See also Refs. [46–50] for discussions of EDMs in THDMs. In addition, it has been shown in Ref. [51] that these CPV phases can be used to realize a successful scenario of the EW baryogenesis. Furthermore, effects of CPV can directly be detected by measuring azimuthal angle distributions in the decay product of additional Higgs bosons [52] at future lepton colliders such as the International Linear Collider (ILC) [53–55], the Circular Electron Positron Collider (CEPC) [56] and the Future Circular Collider (FCC-ee) [57].

In this paper, we study the possibility of direct searches for additional Higgs bosons at LHC in the THDM with the double-alignment. In particular, we focus on the EW pair production of the additional Higgs bosons whose cross sections are simply determined by the masses of the additional Higgs bosons [58–60]. ³ We apply the data for multi-lepton final states at the LHC Run-II experiment to constrain the parameter space of the THDM, and combine constraints from flavor experiments such as $B \rightarrow X_s \gamma$, $B_s \rightarrow \mu\mu$ and leptonic tau decays. Furthermore, we extrapolate the Run-II data to obtain the parameter space expected to be explored at the High-Luminosity LHC (HL-LHC). We find that a large portion of the parameter space has already been excluded by the current LHC data, especially the region being able to be regarded as the Type-X (or lepton specific) THDM.

¹ Such a Higgs doublet can be defined by taking the so-called Higgs basis [21] without loss of generality.

² In this case, non-decoupling effects of additional Higgs bosons can be significant, which provide a sizable deviation in the triple Higgs boson coupling, see e.g., Refs. [23–27]. Such a large deviation can be probed in the double Higgs boson production at future colliders [28–42].

³ In Ref. [61], global fits in the Yukawa aligned THDM have been performed, where various flavor data, signal strengths of the discovered Higgs boson and single productions of the additional Higgs bosons have been combined.

This paper is organized as follows. In Sec. II, we give the Lagrangian of our THDM, and define the double-alignment, i.e., the Yukawa alignment and the Higgs alignment. In Sec. V, we discuss the decays of the additional Higgs bosons. Sec. IV summarizes various constraints from flavor experiments. Sec. V is devoted to show our main results, i.e., parameter regions excluded by the current LHC data and expected to be explored at the HL-LHC. We also demonstrate the reconstruction of masses of additional Higgs bosons from the $b\bar{b}\tau^+\tau^-$ state. Conclusions and discussions are given in Sec. VI. In Appendix, we show the constraint on the parameter space for the special case with $\zeta_u = 0$.

II. MODEL

We consider a model with two isospin Higgs doublets without introducing any symmetry other than the SM gauge symmetry. In this case, the Lagrangian is invariant under the global $U(2)$ transformation between the two doublets by using an appropriate redefinition of parameters in the potential and Yukawa interactions. Using this invariance, we can write down the Lagrangian in terms of the Higgs basis [21] Φ and Φ' without loss of generality, which is defined as

$$\Phi = \begin{pmatrix} G^+ \\ \frac{1}{\sqrt{2}}(v + h_1^0 + iG^0) \end{pmatrix}, \quad \Phi' = \begin{pmatrix} H^+ \\ \frac{1}{\sqrt{2}}(h_2^0 + ih_3^0) \end{pmatrix}, \quad (1)$$

where v is the VEV related to the Fermi constant G_F through $v = (\sqrt{2}G_F)^{-1/2}$. In Eq. (1), G^\pm and G^0 are the Nambu-Goldstone bosons which are absorbed into the longitudinal component of the W^\pm and Z boson, respectively, while H^\pm and h_i^0 ($i = 1, 2, 3$) are the physical charged and neutral Higgs bosons, respectively.

The potential is written in the Higgs basis as

$$V = m^2|\Phi|^2 + M^2|\Phi'|^2 - \left(\mu^2\Phi^\dagger\Phi' + \text{h.c.}\right) + \frac{\lambda_1}{2}|\Phi|^4 + \frac{\lambda_2}{2}|\Phi'|^4 + \lambda_3|\Phi|^2|\Phi'|^2 + \lambda_4|\Phi^\dagger\Phi'|^2 + \left[\frac{\lambda_5}{2}(\Phi^\dagger\Phi') + \lambda_6|\Phi|^2 + \lambda_7|\Phi'|^2\right](\Phi^\dagger\Phi') + \text{h.c.}, \quad (2)$$

where μ^2 and $\lambda_{5,6,7}$ are complex in general. The tadpole conditions, vanishment of the linear term of h_i^0 , provide

$$m^2 = \frac{1}{2}\lambda_1 v^2, \quad \mu^2 = \frac{1}{2}\lambda_6 v^2. \quad (3)$$

We note that the second equation is given by the conditions with respect to h_2^0 or h_3^0 . By imposing the tadpole condition, the squared mass of H^\pm is given by

$$m_{H^\pm}^2 = M^2 + \frac{1}{2}\lambda_3 v^2. \quad (4)$$

The squared-mass matrix for the neutral Higgs bosons in the basis of (h_1^0, h_2^0, h_3^0) is given by

$$\mathcal{M}^2 = v^2 \begin{pmatrix} \lambda_1 & \text{Re}[\lambda_6] & -\text{Im}[\lambda_6] \\ \text{Re}[\lambda_6] & \frac{M^2}{v^2} + \frac{1}{2}(\lambda_3 + \lambda_4 + \text{Re}[\lambda_5]) & -\frac{1}{2}\text{Im}[\lambda_5] \\ -\text{Im}[\lambda_6] & -\frac{1}{2}\text{Im}[\lambda_5] & \frac{M^2}{v^2} + \frac{1}{2}(\lambda_3 + \lambda_4 - \text{Re}[\lambda_5]) \end{pmatrix}. \quad (5)$$

The mass eigenstates H_i^0 ($i = 1, 2, 3$) can be defined by introducing the orthogonal matrix R as $h_i^0 = O_{ij}H_j^0$ with the eigenvalues $\text{diag}(m_{H_1^0}^2, m_{H_2^0}^2, m_{H_3^0}^2) \equiv O^T \mathcal{M}^2 O$. We define $m_{H_1^0} \leq m_{H_2^0} \leq m_{H_3^0}$, and identify the H_1^0 state with the discovered Higgs boson with the mass of 125 GeV.

In this paper, we impose the alignment condition:

$$\lambda_6 = 0, \quad (6)$$

by which the h_1^0 state coincides with the mass eigenstate H_1^0 , and as a result couplings of H_1^0 to the gauge bosons and fermions agree with those of the SM Higgs boson at tree level. We refer this condition as ‘‘Higgs alignment’’. By rephasing Φ' , the complex phase of λ_5 can be removed without loss of generality, so that the mass matrix becomes diagonal form. We note that at this stage we cannot identify the additional Higgs boson H_2^0 (H_3^0) with the CP-even (CP-odd) state, because its CP property depends on the structure of the Yukawa interaction.

In this scenario, there are 7 free parameters⁴ which can be chosen as follows

$$M^2, m_{H_2^0}, m_{H_3^0}, m_{H^\pm}, \lambda_2, |\lambda_7| \text{ and } \theta_7, \quad (7)$$

where $\theta_7 \equiv \arg[\lambda_7] \in (-\pi, \pi]$.

The most general Yukawa interactions are given in the mass eigenstates of fermions as

$$\begin{aligned} \mathcal{L}_Y = & -\bar{Q}_L^u \left(\sqrt{2} \frac{M_u}{v} \tilde{\Phi} + \rho_u \tilde{\Phi}' \right) u_R - \bar{Q}_L^d \left(\sqrt{2} \frac{M_d}{v} \Phi + \rho_d \Phi' \right) d_R \\ & - \bar{L}_L \left(\sqrt{2} \frac{M_e}{v} \Phi + \rho_e \Phi' \right) e_R + \text{h.c.}, \end{aligned} \quad (8)$$

where $Q_L^u = (u_L, V_{\text{CKM}} d_L)^T$, $Q_L^d = (V_{\text{CKM}}^\dagger u_L, d_L)^T$ and $L_L = (\nu_L, e_L)$ are left-handed doublet fermions with V_{CKM} being the Cabibbo-Kobayashi-Maskawa (CKM) matrix, while u_R , d_R and e_R are right-handed up-type quarks, down-type quarks and charged leptons, respectively. The charge conjugation of the Higgs doublets is denoted as $\tilde{\Phi}^{(\prime)} = i\tau_2 \Phi^{(\prime)*}$. In the first term of each parentheses, M_f ($f = u, d, e$) denote diagonalized mass matrices, while in the second term ρ_f represent arbitrary 3×3 complex matrices. In this expression, we do not explicitly show flavor indices.

⁴ The number of parameters can consistently be counted as follows: 14 (initial number of real parameters in the potential) – 3 (tadpole conditions) – 2 (Higgs alignment) – 1 (rephasing) = 7 [Eq. (7)] + 1 ($m_{H_1^0} = 125$ GeV).

It is clear that the ρ_f terms give rise to tree-level FCNCs mediated by neutral Higgs bosons, particularly via H_2^0 and/or H_3^0 in the Higgs alignment limit defined in Eq. (6). In order to avoid such FCNCs, we impose so-called the Yukawa alignment [18], i.e.,

$$\rho_f = \sqrt{2}\zeta_f \frac{M_f}{v}, \quad (9)$$

where ζ_f are arbitrary complex parameters. The Yukawa alignment can also be described in the general basis of the two doublets as the assumption that two Yukawa matrices for a fermion type f are proportional to each other. We note that the ζ_f parameters are flavor universal, e.g., $\zeta_\mu = \zeta_\tau = \zeta_e$, due to the above assumption. Because the ζ_f parameters are complex, new sources of the CPV appear in addition to the potential parameter λ_7 . In Ref. [43], it has been shown that we can take sizable CPV phases, while severe constraints from experiments of the electron EDM [44] and the neutron EDM [45] can be avoided by using cancellation among Barr-Zee diagrams [62] with fermion and scalar boson loops due to the independent phases from Yukawa interactions and the Higgs potential. Such a scenario is compatible with constraints from the other flavor experiments as well as the current LHC data. We note that in THDMs with a softly-broken Z_2 symmetry [14] these ζ_f parameters are determined by one parameter $\tan \beta$ (the ratio of the two Higgs VEVs) depending on the type of Yukawa interactions [16, 17] by

$$\begin{aligned} (\zeta_u, \zeta_d, \zeta_e) &= (\cot \beta, \cot \beta, \cot \beta) && \text{in Type-I,} \\ (\zeta_u, \zeta_d, \zeta_e) &= (\cot \beta, -\tan \beta, -\tan \beta) && \text{in Type-II,} \\ (\zeta_u, \zeta_d, \zeta_e) &= (\cot \beta, \cot \beta, -\tan \beta) && \text{in Type-X,} \\ (\zeta_u, \zeta_d, \zeta_e) &= (\cot \beta, -\tan \beta, \cot \beta) && \text{in Type-Y.} \end{aligned} \quad (10)$$

In the Higgs and Yukawa alignment, the double-alignment, the Higgs boson couplings are expressed as follows

$$\begin{aligned} \mathcal{L}_{\text{int}} = & - \sum_{f=u,d,e} \bar{f} \frac{M_f}{v} [H_1^0 + |\zeta_f|(\cos \theta_f + i \sin \theta_f \gamma_5)H_2^0 + 2I_f|\zeta_f|(\sin \theta_f - i \cos \theta_f \gamma_5)H_3^0] f \\ & - \frac{\sqrt{2}}{v} \bar{u} \left(P_R \zeta_d V_{\text{CKM}} M_d - P_L \zeta_u^* M_u^\dagger V_{\text{CKM}}^\dagger \right) d H^+ - \frac{\sqrt{2}}{v} \bar{\nu} (P_R \zeta_e M_e) e H^+ + \text{h.c.}, \end{aligned} \quad (11)$$

where $\theta_f \equiv \arg[\zeta_f] \in (-\pi, \pi]$, $I_u = 1/2$, $I_d = I_e = -1/2$ and P_L (P_R) is the projection operator for left- (right) handed fermions. It is clear that non-zero phases θ_f result in the CP mixing in the Yukawa sector. We note that the $H_1^0 VV$ ($V = W, Z$) couplings coincide with the SM values at tree level due to the Higgs alignment while $H_{2,3}^0 VV$ couplings vanish. On the other hand, there are Higgs-Higgs-Gauge type interactions for the additional Higgs bosons such as $H_2^0 H_3^0 Z$ and

$H_{2,3}^0 H^\pm W^\mp$, which is phenomenologically important for the EW pair productions of the additional Higgs bosons and their decays as discussed in the following sections.

III. DECAYS OF THE ADDITIONAL HIGGS BOSONS

We discuss decays of additional Higgs bosons in the double-alignment limit, where they can mainly decay into a fermion pair or a lighter additional Higgs boson with a gauge boson as long as these are kinematically allowed. In the following discussion, we focus on the case where the charged Higgs boson mass is degenerate with one of the additional neutral Higgs bosons in order to avoid the T parameter constraint [63–67]. In this case, there are two possible scenarios denoted as the light H^\pm scenario: $m_{H^\pm} = m_{H_2^0}$ and the heavy H^\pm scenario: $m_{H^\pm} = m_{H_3^0}$, where we define $m_{H_3^0} \geq m_{H_2^0} \geq m_{H_1}$ as mentioned in Sec. II.

The decay rates of the Higgs bosons into a fermion pair are given by

$$\Gamma(H_{2,3}^0 \rightarrow f\bar{f}) = \frac{\sqrt{2}G_F m_{H_{2,3}}^3}{8\pi} N_f^c x_f |\zeta_f|^2 [1 - 2x_f(1 \pm \cos 2\theta_f)] \lambda^{1/2}(x_f, x_f), \quad (12)$$

$$\begin{aligned} \Gamma(H^\pm \rightarrow ff') &= \frac{\sqrt{2}G_F m_{H^\pm}^3}{8\pi} |V_{\text{CKM}}^{ff'}|^2 N_f^c \lambda^{1/2}(x_f, x_{f'}) \\ &\times [(x_f |\zeta_f|^2 + x_{f'} |\zeta_{f'}|^2)(1 - x_f - x_{f'}) + 4x_f x_{f'} \text{Re}(\zeta_f^* \zeta_{f'})], \end{aligned} \quad (13)$$

where $\lambda(x, y) = (1 - x - y)^2 - 4xy$, $x_i = m_i^2/m_{\mathcal{H}}^2$ with $m_{\mathcal{H}}$ being the mass of the decaying Higgs boson and $N_f^c = 3(1)$ for f being quarks (leptons). As we mentioned in Sec. II, ζ_f factors are assumed to be flavor universal, e.g., $\zeta_\mu = \zeta_\tau = \zeta_e$. For the case with non-zero mass differences among the additional Higgs bosons, the following decay rates have to be added to their total widths:

$$\Gamma(H_3^0 \rightarrow \phi V^{(*)}) = \begin{cases} \frac{\sqrt{2}G_F m_{H_3^0}^3}{16\pi} \lambda^{3/2}(x_\phi, x_V) & (m_{H_3^0} - m_\phi \geq m_V) \\ \frac{9m_{H_3^0}}{16\pi^3} G_F^2 m_V^4 \delta_V G(x_\phi, x_V) & (m_{H_3^0} - m_\phi < m_V) \end{cases}, \quad (14)$$

$$\Gamma(H^\pm \rightarrow H_2^0 W^{\pm(*)}) = \begin{cases} \frac{\sqrt{2}G_F m_{H^\pm}^3}{16\pi} \lambda^{3/2}(x_{H^\pm}, x_W) & (m_{H^\pm} - m_{H_2^0} \geq m_W) \\ \frac{9m_{H^\pm}}{16\pi^3} G_F^2 m_W^4 G(x_{H_2}, x_W) & (m_{H^\pm} - m_{H_2^0} < m_W) \end{cases}, \quad (15)$$

where ⁵ $\phi = H_2^0 (H^\pm)$ for $V^{(*)} = Z^{(*)} (W^\mp)^{(*)}$, $\delta_W = 1$ and $\delta_Z = \frac{7}{6} - \frac{20}{9} \sin^2 \theta_W + \frac{80}{27} \sin^4 \theta_W$. The function G is the phase space function for three body decays, see e.g., Ref. [68] for the explicit form of this function:

$$G(x, y) = \frac{1}{12y} \left\{ 2(x-1)^3 - 9(x^2-1)y + 6(x-1)y^2 - 3 \left[1 + (x-y)^2 - 2y \right] y \log x \right.$$

⁵ In Eq. (14) with $\phi = H^\pm$ and $V = W$, this expression does not take the sum over two possible states, i.e., $H^+ W^{-(*)}$ and $H^- W^{+(*)}$.

$$+ 6(1+x-y)y\sqrt{-\lambda(x,y)} \left[\arctan\left(\frac{-1+x-y}{\sqrt{-\lambda(x,y)}}\right) + \arctan\left(\frac{-1+x+y}{\sqrt{-\lambda(x,y)}}\right) \right] \}. \quad (16)$$

We note that loop induced decays of the additional neutral Higgs bosons, i.e., $H_{2,3}^0 \rightarrow gg/\gamma\gamma/Z\gamma$ are also taken into account in numerical evaluations, while those of the charged Higgs boson, i.e., $H^\pm \rightarrow W^\pm\gamma$ [69] and $H^\pm \rightarrow W^\pm Z$ [70] are neglected because of their tiny partial widths.

As we mentioned in the above, the decay modes of H_3^0 can be classified into two categories, i.e., fermionic modes ($H_3^0 \rightarrow f\bar{f}$) and bosonic modes ($H_3^0 \rightarrow \phi V^{(*)}$). The relative size of the branching ratios for the fermionic and bosonic modes can be expressed by introducing the following ratio R :

$$R \equiv \frac{\sum_f \Gamma(H_3^0 \rightarrow f\bar{f})}{\sum_f \Gamma(H_3^0 \rightarrow f\bar{f}) + \sum_V \Gamma(H_3^0 \rightarrow \phi V^{(*)})} \simeq \sum_f \mathcal{B}(H_3^0 \rightarrow f\bar{f}). \quad (17)$$

In addition, we introduce

$$R_\tau \equiv \frac{\Gamma(H_3^0 \rightarrow \tau^+\tau^-)}{\sum_f \Gamma(H_3^0 \rightarrow f\bar{f})}, \quad (18)$$

by which we can parameterize the relative magnitude of the branching ratio of $H_3^0 \rightarrow \tau^+\tau^-$ among the fermionic modes. These R parameters can simply be rewritten as

$$R = \frac{1}{1+r/\zeta^2}, \quad R_\tau = \frac{|\zeta_e|^2}{\zeta^2}, \quad (19)$$

where

$$\zeta^2 = \frac{\sum_f \Gamma(H_3^0 \rightarrow f\bar{f})}{\Gamma_0}, \quad \Gamma_0 = \frac{\sqrt{2}G_F}{8\pi} m_{H_3^0} m_\tau^2, \quad (20)$$

$$r = \begin{cases} \frac{m_{H_3^0}^2}{2m_\tau^2} \sum_{V,\phi} \lambda^{3/2} \left(\frac{m_\phi^2}{m_{H_3^0}^2}, \frac{m_V^2}{m_{H_3^0}^2} \right) & (m_{H_3^0} - m_\phi \geq m_V) \\ \frac{9}{2\sqrt{2}\pi^2} \frac{G_F}{m_\tau^2} \sum_{V,\phi} m_V^4 \delta_V G \left(\frac{m_\phi^2}{m_{H_3^0}^2}, \frac{m_V^2}{m_{H_3^0}^2} \right) & (m_{H_3^0} - m_\phi < m_V), \end{cases} \quad (21)$$

with the summation $\sum_{V,\phi}$ being taken to be $(V, \phi) = (Z, H_3^0)$ and (W, H^\pm) . In particular, for the case with $m_b \ll m_{H_{2,3}} < 2m_t$, which will be mainly considered in Sec. V, ζ^2 takes a significantly simple form as

$$\zeta^2 \simeq \frac{1}{m_\tau^2} \sum_{f \neq t} m_f^2 N_f^c |\zeta_f|^2. \quad (22)$$

We note that H_2^0 can only decay into a fermion pair at tree level, so that the R value for H_2^0 , i.e., $R|_{H_3^0 \rightarrow H_2^0}$ is unity.

Similar to the neutral Higgs bosons, we define the ratio parameters for H^\pm as follows:

$$R^\pm \equiv \frac{\sum_f \Gamma(H^\pm \rightarrow f\bar{f}')}{\sum_f \Gamma(H^\pm \rightarrow f\bar{f}') + \Gamma(H^\pm \rightarrow H_2^0 W^\pm)} \simeq \sum_f \mathcal{B}(H^\pm \rightarrow f\bar{f}'), \quad (23)$$

$$R_\tau^\pm \equiv \frac{\Gamma(H^\pm \rightarrow \tau\nu)}{\sum_f \Gamma(H^\pm \rightarrow f\bar{f}')}. \quad (24)$$

By introducing the quantities ζ_\pm^2 and r_\pm , these R parameters can be expressed as

$$R^\pm = \frac{1}{1 + r_\pm/\zeta_\pm^2}, \quad R_\tau^\pm = \frac{|\zeta_e|^2}{\zeta_\pm^2}, \quad (25)$$

where

$$\zeta_\pm^2 = \frac{\sum_f \Gamma(H^\pm \rightarrow f\bar{f}')}{\Gamma_0|_{H_3^0 \rightarrow H^\pm}} \simeq |\zeta_e|^2 + 3 \left(1 - \frac{m_t^2}{m_{H^\pm}^2}\right)^2 \left(\frac{m_t^2}{m_\tau^2} |\zeta_u|^2 + \frac{m_b^2}{m_\tau^2} |\zeta_d|^2\right), \quad (26)$$

$$r_\pm = \begin{cases} \frac{m_{H^\pm}^2}{2m_\tau^2} \lambda^{3/2} \left(\frac{m_{H_2^0}^2}{m_{H^\pm}^2}, \frac{m_W^2}{m_{H^\pm}^2}\right) & (m_{H^\pm} - m_{H_2^0} \geq m_W) \\ \frac{9}{2\sqrt{2}\pi^2} \frac{G_F}{m_\tau^2} m_W^4 G \left(\frac{m_{H_2^0}^2}{m_{H^\pm}^2}, \frac{m_W^2}{m_{H^\pm}^2}\right) & (m_{H^\pm} - m_{H_2^0} < m_W) \end{cases}, \quad (27)$$

Unlike the H_3^0 decays, only the decay of $H^\pm \rightarrow H_2^0 W^{\pm(*)}$ is allowed for the bosonic decay mode.

In terms of these R parameters, the decay branching ratios into a tau lepton pair, which will be important in the discussion for the phenomenology at LHC, can simply be expressed as

$$\mathcal{B}(H_2^0 \rightarrow \tau^+\tau^-) \simeq R_\tau, \quad \mathcal{B}(H_3^0 \rightarrow \tau^+\tau^-) \simeq RR_\tau, \quad \mathcal{B}(H^\pm \rightarrow \tau^\pm\nu) \simeq R^\pm R_\tau^\pm. \quad (28)$$

It would be important to discuss the critical values of ζ and ζ_\pm which give the sum of the fermionic decay branching ratios to be 50%. Such critical values, denoted as ζ_{50} and $\zeta_{\pm 50}$, can be expressed as $\zeta_{50} = \sqrt{r}$ and $\zeta_{\pm 50} = \sqrt{r_\pm}$ from Eqs. (19) and (25), respectively. Since r and r_\pm depend only on the masses of additional Higgs bosons, ζ_{50} and $\zeta_{\pm 50}$ are determined as a function of these masses.

Fig. 1 shows the values of ζ_{50} (left panel) and $\zeta_{\pm 50}$ (right panel) as a function of $m_{H_3^0} - m_{H_2^0}$. We see that for $m_{H_3^0} - m_{H_2^0} \ll m_W$ both ζ_{50} and $\zeta_{\pm 50}$ are much smaller than unity, because the bosonic decay modes are significantly suppressed by the phase space, while they can be of order one for $m_{H_3^0} - m_{H_2^0} \sim m_W$. When the on-shell decays open, ζ_{50} and $\zeta_{\pm 50}$ are of order 10 or larger. We also see that ζ_{50} and $\zeta_{\pm 50}$ almost do not depend on $m_{H_3^0}$, so that they are essentially determined by the mass difference $m_{H_3^0} - m_{H_2^0}$. It is clear that larger values of ζ_{50} are required for $m_{H^\pm} = m_{H_2^0}$ (dashed curves) as compared with that with $m_{H^\pm} = m_{H_3^0}$ (solid curves), because the $H_3^0 \rightarrow H^\pm W^{\pm(*)}$ mode also contribute to the r value.

Similarly, we discuss the critical values of ζ_f which lead to $R_\tau = 50\%$ or $R_\tau^\pm = 50\%$. From Eqs. (19) and (25), R_τ and R_τ^\pm are determined by the ratios of the ζ_f parameters, i.e., ζ_u/ζ_e and ζ_d/ζ_e . More concretely, the inverse of R_τ and R_τ^\pm can be expressed for $\theta_f = 0$ as

$$R_\tau^{-1} \simeq 1 + \frac{3m_b^2 |\zeta_d|^2}{m_\tau^2 |\zeta_e|^2} + \left[\frac{3m_c^2}{m_\tau^2} + \theta_{tt} \frac{3m_t^2}{m_\tau^2} \left(1 - \frac{4m_t^2}{m_{H_3^0}^2}\right)^{3/2} \right] \frac{|\zeta_u|^2}{|\zeta_e|^2}, \quad (29)$$

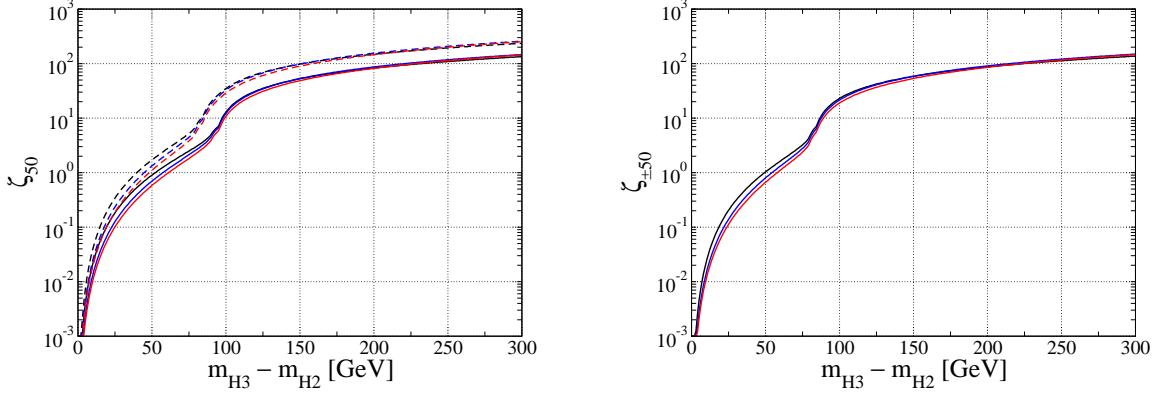


FIG. 1. Values of ζ_{50} (left) and $\zeta_{\pm 50}$ (right) as a function of the mass difference $m_{H_3} - m_{H_2}$ for $m_{H_2^0} = 100$ GeV (black), 300 GeV (blue) and 500 GeV (red). For the left panel, the solid and dashed curves show the case with the heavy ($m_{H^\pm} = m_{H_3^0}$) and the light ($m_{H^\pm} = m_{H_2^0}$) H^\pm scenario, respectively.

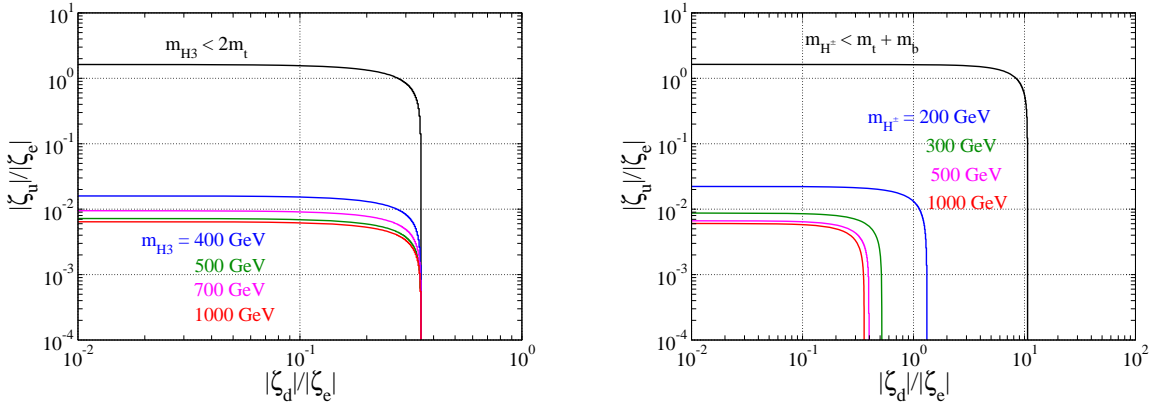


FIG. 2. Contour plots for $R_\tau = 50\%$ (left) and $R_\tau^\pm = 50\%$ (left) on the $|\zeta_d|/|\zeta_e|$ and $|\zeta_u|/|\zeta_e|$ plane for each fixed value of $m_{H_2^0}$ (left) and m_{H^\pm} (right).

$$(R_\tau^\pm)^{-1} \simeq 1 + \left[\frac{3m_s^2}{m_\tau^2} + \theta_{tb} \frac{3m_b^2}{m_\tau^2} \left(1 - \frac{m_t^2}{m_{H^\pm}^2} \right)^2 \right] \frac{|\zeta_d|^2}{|\zeta_e|^2} + \left[\frac{3m_c^2}{m_\tau^2} + \theta_{tb} \frac{3m_t^2}{m_\tau^2} \left(1 - \frac{m_t^2}{m_{H^\pm}^2} \right)^2 \right] \frac{|\zeta_u|^2}{|\zeta_e|^2}, \quad (30)$$

where $\theta_{tt} \equiv \theta(m_{H_3^0} - 2m_t)$ and $\theta_{tb} \equiv \theta(m_{H^\pm} - m_t - m_b)$ with $\theta(x)$ being the Heaviside step function. These expressions show that the values of $(R_\tau)^{-1} - 1$ and $(R_\tau^\pm)^{-1} - 1$ obey the equation of an ellipse with the x (y) axis corresponding to $|\zeta_d|/|\zeta_e|$ ($|\zeta_u|/|\zeta_e|$). This is numerically shown in Fig. 2. Here, we show the first quadrant of the ellipse. The points on each curve represent the required values of $|\zeta_d|/|\zeta_e|$ and $|\zeta_u|/|\zeta_e|$ to obtain $R_\tau = 50\%$ (left panel) and $R_\tau^\pm = 50\%$ (right panel). For the case below the top threshold, the curve almost does not depend on $m_{H_2^0}$, and the interceptions of x and

m_t [GeV]	m_b [GeV]	m_c [GeV]	m_Z [GeV]	m_W [GeV]	m_{H_1} [GeV]	$\alpha_s(m_Z)$	α_{em}^{-1}	
172.76 [71]	4.561 [72]	1.092 [72]	91.1876 [71]	80.379 [71]	125.25 [71]	0.1182 [73]	137.036 [71]	
$\mathcal{B}(\bar{B} \rightarrow X_c \ell^- \nu)$	$ V_{ts}^* V_{tb}/V_{cb} ^2$	$ V_{cb} $	$\bar{\tau}(B_s^0)$ [ps]	$\tau(B_{sL}^0)$ [ps]	$\tau(B_{sH}^0)$ [ps]	$\Delta\Gamma_s$ [ps $^{-1}$]	m_{B_s} [GeV]	f_{B_s} [GeV]
0.1065 [74]	0.9626 [75, 76]	0.041 [75]	1.510 [74]	1.414 [74]	1.619 [74]	0.090 [74]	5.367 [71]	0.2284 [73]

TABLE I. Input SM parameters. We take the central values of these parameters.

y axis are simply determined by the fermion mass ratio extracted from Eqs. (29) and (30), i.e., $|\zeta_d|/|\zeta_e| \simeq m_\tau/(\sqrt{3}m_b) \simeq 0.35$ and $|\zeta_u|/|\zeta_e| \simeq m_\tau/(\sqrt{3}m_c) \simeq 1.6$. On the other hand, above the top threshold, the dependence of $m_{H_2^0}$ slightly appears due to the phase function as seen in Eqs. (29) and (30). For R_τ^\pm (right panel), both the $|\zeta_d|/|\zeta_e|$ and $|\zeta_u|/|\zeta_e|$ depend on $m_{H_2^0}$, because the phase space suppression is multiplied to both the $|\zeta_d|^2/|\zeta_e|^2$ and $|\zeta_u|^2/|\zeta_e|^2$ terms for $m_{H^\pm} > m_t + m_b$.

By looking at Figs. 1 and 2 and using Eq. (28), the Higgs boson decays into a tau lepton pair can well be estimated.

IV. FLAVOR CONSTRAINTS

In our scenario, the additional Higgs bosons can mediate various flavor processes and change their predictions from those in the SM. Such effects can be translated into constraints on the masses of Higgs bosons and the ζ_f parameters, defined in Sec. II.

Let us first discuss the constraint from $B \rightarrow X_s \gamma$ decay process. The current experimental value of the branching ratio is given by [74]

$$\mathcal{B}(B \rightarrow X_s \gamma) = (3.32 \pm 0.15) \times 10^{-4}. \quad (31)$$

In THDMs, the charged Higgs boson can run in the one-loop diagram instead of the W boson, so that there is a sensitivity to m_{H^\pm} and quark Yukawa couplings which correspond to ζ_u and ζ_d in our scenario. It has been known that QCD corrections can sizably change the prediction, e.g., about a few 10% at NLO with respect to the LO prediction in the SM [77]. The NNLO QCD corrections have also been calculated in Ref. [78] in the THDM. We implement the NLO QCD and QED corrections to the decay rate according to Ref. [79] and [80], respectively.⁶ The constraint from $B \rightarrow X_s \gamma$ is particularly important for larger values of ζ_u which correspond to the case with a smaller $\tan \beta$ value in the THDMs with the softly-broken Z_2 symmetry, see e.g., [78].

⁶ We set the renormalization scale of the B meson decay μ_b to be the pole mass of the bottom quark m_b , while that of the matching to the full EW theory to be m_W .

In addition to $B \rightarrow X_s \gamma$, we take into account the constraint from $B_s \rightarrow \mu\mu$ decay. The current experimental value of the branching ratio is given by [74]

$$\mathcal{B}(B_s \rightarrow \mu\mu) = (3.1 \pm 0.6) \times 10^{-9}. \quad (32)$$

In the aligned THDM, the charged Higgs boson can contribute to the process via box and penguin type diagrams. The latter also contains neutral Higgs exchanges. Unlike the $B \rightarrow X_s \gamma$ process, the $B_s \rightarrow \mu\mu$ process has a sensitivity to the masses of neutral Higgs bosons and the ζ_e parameters in addition to m_{H^\pm} , ζ_u and ζ_d . Therefore, even in a case with smaller ζ_u which is not excluded by $B \rightarrow X_s \gamma$, scenarios with larger ζ_d and/or ζ_e can be excluded. We implement the decay rate of $B_s \rightarrow \mu\mu$ at one-loop level according to Ref. [81] by utilizing the Wilson coefficient $C_{10}(\bar{s}\gamma_\mu P_L b)(\bar{\mu}\gamma^\mu\gamma_5\mu)$ in the SM evaluated at NNLO of QCD as [82]

$$C_{10}^{\text{SM}} = -0.938 \times \left(\frac{m_t}{173.1 \text{ GeV}}\right)^{1.53} \times \left(\frac{\alpha_s(m_Z)}{0.1184}\right)^{-0.09}. \quad (33)$$

Finally, we take into account the leptonic tau decays which are mediated by the charged Higgs boson in addition to the contribution from the W boson at tree level. Thus, the combination of $\zeta_e^2/m_{H^\pm}^2$ is constrained [83]. Because the coupling of H^\pm with an electron is negligibly small, the contributions of H^\pm to $\tau \rightarrow e\nu_\tau\bar{\nu}_e$ and $\mu \rightarrow e\nu_\mu\bar{\nu}_e$ are negligible. This causes the violation of lepton flavor universality, which has been stringently constrained by experiments. The current world average is [74]

$$(g_\tau/g_\mu)_{\text{ave}} = 0.9999 \pm 0.0014. \quad (34)$$

The left-hand side of the above expression can be compared with the theory prediction of $\Gamma(\tau \rightarrow \mu\nu_\tau\bar{\nu}_\mu)_{\text{THDM}}/\Gamma(\tau \rightarrow \mu\nu_\tau\bar{\nu}_\mu)_{\text{SM}}$.

For numerical evaluations, we use the SM input parameters shown in Table I, and show the parameter region constrained by the flavor data in the next section.

V. DIRECT SEARCHES FOR ADDITIONAL HIGGS BOSONS AT LHC

We discuss constraints on the model parameters from direct searches for the additional Higgs bosons by using the current LHC data in the double-aligned THDM. We also study the parameter space expected to be explored at the HL-LHC. For simplicity, we here consider the CP-conserving case, i.e., $\theta_f = 0$, in which the constraint from LHC data almost does not depend on these phases while that from flavor experiments discussed in the previous section has a sensitivity to these

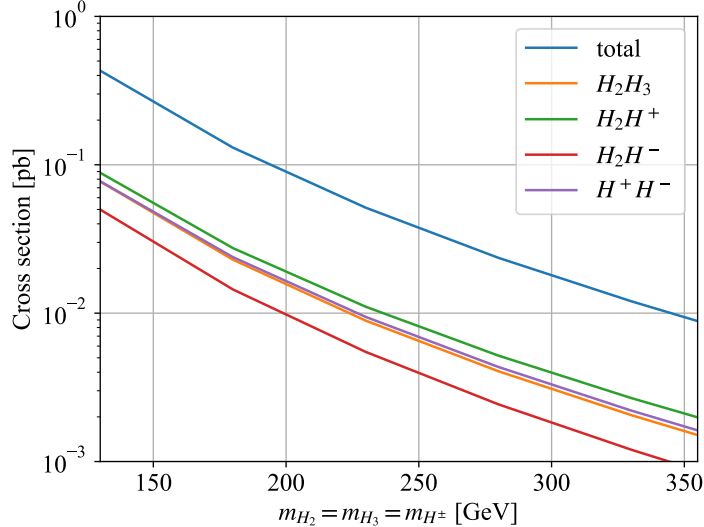


FIG. 3. Cross sections for the EW pair production of the additional Higgs bosons at LHC with the collision energy of 13 TeV as a function of the degenerate masses $m_{H_2^0}(=m_{H_3^0}=m_{H^\pm})$.

phases. In addition, we concentrate on the case where the additional neutral Higgs bosons are lighter than $2m_t$ as the phenomenologically interesting region.

We particularly focus on the EW pair production of the additional Higgs bosons. The cross sections of these processes are simply determined by the gauge coupling for fixed Higgs boson masses [58–60], so that the number of signal events is determined by decays of the Higgs bosons. This is quite different from single Higgs productions such as the gluon fusion process and the bottom or top quark associated process whose cross sections depend on Yukawa couplings. We note that the single additional Higgs boson production associated with a weak boson [84], e.g., $pp \rightarrow H_{2,3}^0 Z$, is absent at tree level in the Higgs alignment limit, so that we do not consider these production modes. Thus, we focus on the EW production, by which we obtain a robust constraint on the masses of the additional Higgs bosons for given decay branching ratios, because the production cross section cannot be tuned to be small by taking model parameters.

A. EW pair productions of the additional Higgs bosons

We study the pair productions of the additional Higgs bosons. There are the following 6 subprocesses [59, 85–87]:

$$pp \rightarrow H_2^0 H_3^0, \quad pp \rightarrow H_2^0 H^\pm, \quad pp \rightarrow H_3^0 H^\pm, \quad pp \rightarrow H^+ H^-. \quad (35)$$

Fig. 3 shows the total cross section of the EW pair production at LO in the unit of pb as a

function of the additional Higgs boson mass, where $m_{H_2^0} = m_{H_3^0} = m_{H^\pm}$ is assumed. We also show the cross sections of each subprocess. As we see in this plot, the cross section can be of $\mathcal{O}(10 - 500)$ fb at LHC with 13 TeV for $m_{H_2^0}, m_{H_3^0} \lesssim 350$ GeV. Thus, $\mathcal{O}(10^3 - 10^5)$ events are already expected even in the current LHC data with the integrated luminosity of 139 fb^{-1} , and we would expect $\mathcal{O}(10^4 - 10^6)$ events are produced at the HL-LHC with 3 ab^{-1} .⁷

As we discussed in Sec. III, the ζ_f parameters control the branching ratios of the additional Higgs bosons. Especially, the leptonic branching ratios are described through the four R parameters; R , R_τ , R^\pm and R_τ^\pm , see Eq. (28). The ζ_f dependence of the model then appears in the signal cross sections including the decay of the Higgs boson, which can be expressed as

$$\sigma(pp \rightarrow AB \rightarrow i_A i_B) \sim \sigma(pp \rightarrow AB) \cdot \mathcal{B}(A \rightarrow i_A) \cdot \mathcal{B}(B \rightarrow i_B), \quad (36)$$

where A and B are H_2^0 , H_3^0 or H^\pm . Their decay modes including the subsequent additional Higgs decay modes are indicated by i_A and i_B . For example, $i_{H_3^0} = \{\tau^+\tau^-, b\bar{b}, Z^{(*)}\tau^+\tau^-, Z^{(*)}b\bar{b}, W^{\pm(*)}\tau^\mp\nu, W^{\pm(*)}tb, \dots\}$ and $i_{H^\pm} = \{\tau^\pm\nu, tb, W^{\pm(*)}\tau^+\tau^-, W^{\pm(*)}b\bar{b}, \dots\}$.

When the branching ratios of the additional Higgs bosons into a charged lepton pair are large, multi-tau signatures from the EW pair production can be used to probe such models [88, 89]. We will show that the current multi-lepton searches at LHC provide strong constraints on the model especially when the additional Higgs bosons dominantly decay into charged leptons. We will also show the expected constraint on the parameter space at the HL-LHC by extrapolating these data.

B. Constraints from multi-lepton searches at LHC

We here consider the constraints on the model by the latest multi-lepton searches at LHC reported by the ATLAS collaboration [90].⁸ In this analysis, events with 4 or more leptons including tau leptons have been searched, which are classified into 14 signal regions with different combinations of the requirements on the lepton species, the number of b -tagged jets, and the existence of the lepton pair consistent with a Z -boson decay. For these signal regions, the minimum numbers of isolated electrons, muons, τ -tagged jets and b -tagged jets are required. The following kinematical cuts are imposed for signal events, i.e., $p_T > 7$ GeV, $|\eta| < 2.47$ for electrons $p_T > 5$ GeV, $|\eta| < 2.7$ for muons and $p_T > 20$ GeV, $|\eta| < 2.5$ for jets.

⁷ In this paper, we show the results for 13 TeV although the ultimate planned center of mass energy at HL-LHC is 14 TeV, where about 10-15 % more events are expected for our signals.

⁸ The corresponding analysis by the CMS collaboration utilizes the Neural Network approach [91], which is difficult to interpret in our model, and thus we do not include it.

SR	SR in Ref. [90]	$N(e, \mu)$	$N(\tau_{\text{had}})$	$N(b\text{-jets})$	$m_{\text{eff}}^{\text{th}}$ [GeV]	$N_{\text{obs}}^{\text{BG}}$	$N_{\text{exp}}^{\text{BG}}$	S_{obs}^{95}	S_{exp}^{95}
SR1	SR1 _{bveto} ^{loose}	=3	≥ 1	0	600	7	7.7	6.37	7.46
SR2	SR1 _{bveto} ^{tight}	=3	≥ 1	0	1000	2	1.6	4.47	4.22
SR3	SR1 _{breq}	=3	≥ 1	≥ 1	1300	2	2.2	4.56	4.59
SR4	SR2 _{bveto} ^{loose}	=2	≥ 2	0	600	5	3.4	8.45	7.45
SR5	SR2 _{bveto} ^{tight}	=2	≥ 2	0	1000	2	0.35	5.63	3.53
SR6	SR2 _{breq}	=2	≥ 2	≥ 1	1100	1	0.52	4.17	3.16
SR7	SR5L	=5	≥ 0	≥ 0	–	21	12.4	17.88	9.88

TABLE II. Summary of the relevant SRs and corresponding limits for 139 fb^{-1} quoted from Ref. [90], where $N_{\text{obs}}^{\text{BG}}$ ($N_{\text{exp}}^{\text{BG}}$) is the observed (expected) number of background events and S_{obs}^{95} (S_{exp}^{95}) is the observed (expected) upper limits on the number of signal events at 95% CL.

We find that the seven signal regions among them are relevant to constrain our model, and call the three 3L1T (L: e or μ and T: τ) signal regions defined in the ATLAS analysis as SR1-SR3, the three 2L2T regions as SR4-SR6, and the 5L0T region as SR7. A summary of the definition of the relevant SRs is shown in Table II, where the observed and the expected number of SM backgrounds and that of 95% CL upper bounds for the signal in each SR are also provided. We have checked that the other seven signal regions provide weaker constraints than the seven signal regions considered here, and therefore, they are omitted in the following analysis.

As future prospects at the HL-LHC, we set the constraints on the model parameters based on the assumption with null contribution from new physics. The expected upper limit on the number of signal events is then estimated by using the Poisson distribution, in which we use the expected number of SM events obtained by extrapolating $N_{\text{exp}}^{\text{BG}}$ (expected number of SM events for 139 fb^{-1}) to that given at the HL-LHC, i.e., $N_{\text{exp}}^{\text{BG}} \times 3000/139$. For instance for SR6, the upper limit on the signal event number at 95% CL is given to be about 9.

We perform the simulation study by using `MadGraph5` [92] and `Pythia 8` [93] with the detector simulation using `Delphes3` [94]. We consider the 16 model points with different additional Higgs masses labeled with $0 \leq n_2 \leq n_3 \leq 3$, corresponding to $180 \text{ GeV} \leq m_{H_2^0} \leq m_{H_3^0} \leq 330 \text{ GeV}$, as follows:

$$m_{H_2^0} = 180 + 50n_2 \text{ GeV}, \quad m_{H_3^0} = 180 + 50n_3 \text{ GeV}, \quad m_{H^\pm} = \begin{cases} m_{H_3^0} & (\text{heavy } H^\pm \text{ scenario}) \\ m_{H_2^0} & (\text{light } H^\pm \text{ scenario}) \end{cases}. \quad (37)$$

In our simulation, we fix $\zeta_u = 0.01$, $\zeta_d = 0.1$ and $\zeta_e = 0.5$ for the model points with $|\Delta m| = m_{H_3^0} - m_{H_2^0} \leq 50 \text{ GeV}$, where we define $\Delta m = m_{H^\pm} - m_{\text{no-deg}}$ with $m_{\text{no-deg}}$ being the mass

of the additional neutral Higgs which is not degenerate with m_{H^\pm} . For the model points with $|\Delta m| \geq 100$ GeV, larger ζ_e and ζ_d values are adopted to achieve $R \sim R_\tau \sim 50$ % to keep the several decay modes contribute in a similar size.

For different values of ζ_f , we estimate the number of events falling down in a certain SR by multiplying the scaling factors defined as the ratio of the product of the branching ratios, i.e., $\mathcal{B}(A \rightarrow i_A)\mathcal{B}(B \rightarrow i_B)|_{\zeta_f}/\mathcal{B}(A \rightarrow i_A)\mathcal{B}(B \rightarrow i_B)|_{\text{fixed}}$ with the numerator (denominator) being the value at arbitrary ζ_f (ζ_f fixed to be the above values). We note that the production cross section does not depend on the ζ_f parameters, so that the scaling factor is needed to be multiplied only to the branching ratios as explained in the above.

In Fig. 4, we show the region of the parameter space excluded by the LHC data and flavor experiments at 95 % CL in the ζ_e - ζ_d plane for the case with $(m_{H_2^0}, m_{H_3^0}, m_{H^\pm}) = (230, 280, 280)$ GeV (left panel) and $(230, 280, 230)$ GeV (right panel). These two mass spectra are the representative choices for the heavy H^\pm and the light H^\pm scenarios. The ζ_u parameter is fixed to be 0.1 in these plots. The region below the black-solid (blue-dashed) curves are excluded by using S_{obs}^{95} (S_{exp}^{95}) given in Table II. The red-dotted curve shows the expected exclusion of the parameter space at the HL-LHC (3 ab^{-1}). We note that these excluded regions are obtained by taking into account all the seven SRs defined in Table II. Namely, we draw these curves so as to maximize the area of the excluded region. We find that these constraints are dominantly determined from SR4, where two isolated leptons and at least two τ -tagged jets are required with the lowest m_{eff} threshold $m_{\text{eff}}^{\text{th}} = 600$ GeV. The sensitivity tends to increase as the leptonic (mainly tau) branching ratio increases, so that it is highly correlated to R_τ which is the function of $|\zeta_e/\zeta_d|$ and $|\zeta_e/\zeta_u|$ as shown in Fig. 2. Interestingly, even though the light H^\pm scenario (shown in the right panel) predicts a larger production cross section than the heavy H^\pm case (shown in the left panel), the constraint from the LHC data in the former case is weaker. This is because the heavier H^\pm provide more H_2^0 via the decay $H^\pm \rightarrow W^{\pm(*)}H_2^0$, which give more tau leptons in the final states. More concretely, we find that the current LHC data excludes the region with $\zeta_e/\zeta_d \gtrsim 10$ ($\zeta_e/\zeta_d \gtrsim 20$) for the heavy (light) H^\pm case as long as $\zeta_e \gtrsim 0.1$ ($\zeta_e \gtrsim 3$). These bounds are expected to be significantly improved at the HL-LHC, where the region with $\zeta_e/\zeta_d \gtrsim 2$ can be excluded, shown as the red-dotted curves.

The constraints from the precision measurements of the flavor observables discussed in Sec. IV are also overlaid on these panels. The regions excluded by the measurements of $B \rightarrow X_s \gamma$, $B_s \rightarrow \mu\mu$ and the leptonic τ decay are depicted in the orange, magenta and cyan regions, respectively. In addition, those excluded by the current LHC searches for additional neutral Higgs bosons via the gluon fusion production ($ggH_{2,3}^0$) and the bottom quark associated production $b\bar{b}H_{2,3}^0$ with the

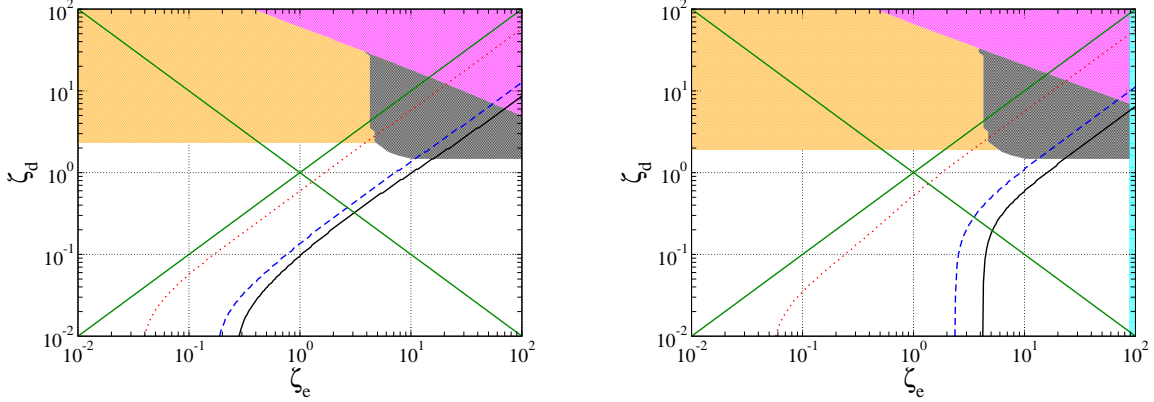


FIG. 4. Constraint on the parameter space on the ζ_e - ζ_d plane in the case with $\zeta_u = 0.1$ for $(m_{H_2^0}, m_{H_3^0}, m_{H^\pm}) = (230, 280, 280)$ GeV in the left panel and $(230, 280, 230)$ GeV in the right panel. The regions below the black-solid, blue-dashed and red-dotted curves are excluded by the observed LHC Run-II data, the expected LHC Run-II data and data expected at the HL-LHC, respectively. The regions shaded by orange, magenta and cyan are excluded by the constraints from $B \rightarrow X_s \gamma$, $B_s \rightarrow \mu\mu$ and the leptonic tau decay, respectively, while those shaded by black are excluded by the searches for $gg \rightarrow H_{2,3}^0 \rightarrow \tau^+ \tau^-$ and $gg \rightarrow b\bar{b}H_{2,3}^0 \rightarrow b\bar{b}\tau^+ \tau^-$ at the LHC Run-II experiments. The green lines indicate the case with $\zeta_d = \zeta_e$ and $\zeta_d = \zeta_e^{-1}$.

subsequent $H_{2,3} \rightarrow \tau^+ \tau^-$ decay [95] are depicted by the black regions. We note that the flavor constraints are sensitive to the signs (complex phases) of the ζ_f parameters while the constraints from the LHC multi-lepton searches are essentially insensitive to those. We see that $B \rightarrow X_s \gamma$ sets the upper limit on the value of ζ_d to be about 2, which does not depend on ζ_e . On the other hand, the constraint from the single Higgs productions (black shaded region) excludes the region with larger values of ζ_e and ζ_d , in which the exclusion is almost given only by the $pp \rightarrow b\bar{b}H_{2,3}^0 \rightarrow b\bar{b}\tau^+ \tau^-$ channel. The region with $\zeta_e \gtrsim \mathcal{O}(100)$ is excluded by the leptonic tau decay. No further region is excluded by the $B_s \rightarrow \mu\mu$ data in this setup. As a summary of this figure, we clarify that except for the bottom-left region i.e., $\zeta_e/\zeta_d \lesssim \mathcal{O}(1)$ with $\zeta_d \lesssim \mathcal{O}(1)$, most of the parameter region can be excluded or explored after combining all the constraints (including the expected bound from the HL-LHC) considered in this section.

C. Dependence on the masses of the additional Higgs bosons

We discuss the constraints on the parameter space for the different 16 mass spectra defined in Eq. (37) in order to see the mass dependence of the constraints. Figs. 5 and 6 respectively show

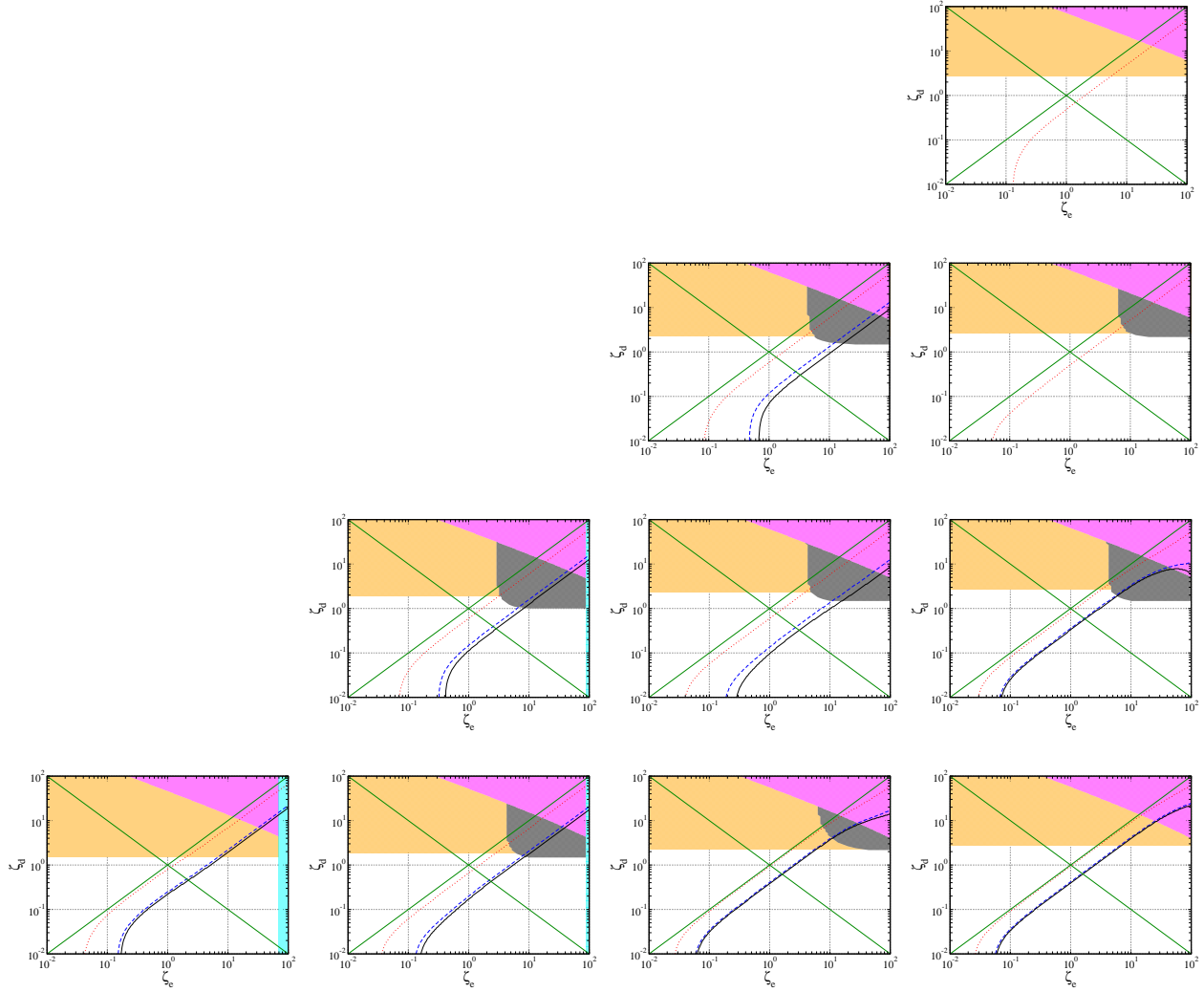


FIG. 5. Constraint on the parameter space on the ζ_e - ζ_d plane for $\zeta_u = 0.1$ in the heavy H^\pm scenario ($m_{H^\pm} = m_{H_3^0} \geq m_{H_2^0}$). The bottom to top panels show the case with $m_{H_2^\pm} = 180, 230, 280$ and 330 GeV while the most left panels show the case with $|\Delta m| (= m_{H_3^0} - m_{H_2^0}) = 0$, and next panels show the case incrementing Δm with a step of 50 GeV (up to $m_{H_3^0} = 330$ GeV). In each panel, the descriptions of curves and shaded regions are the same as those given in Fig. 4.

the results for the heavy H^\pm scenario and the light H^\pm scenario. The descriptions for each curve and shaded region are the same as those explained in Fig. 4.

In Fig. 5, we see that slightly larger regions are excluded for the case with $|\Delta m| \neq 0$ as compared to that with $|\Delta m| = 0$ for $m_{H_2^\pm} = 180$ GeV (bottom panels) and 230 GeV (next to bottom panels). This can be understood by the effect of the $H^\pm \rightarrow W^{\pm(*)}H_2^0 \rightarrow \tau^+\tau^-$, providing more tau leptons at final states. We note that the decay of $H^\pm \rightarrow W^{\pm(*)}H_2^0$ is suppressed for larger values of ζ_e and/or ζ_d due to the enhancement of the $H^\pm \rightarrow \tau\nu$ and $H^\pm \rightarrow tb$ modes, so

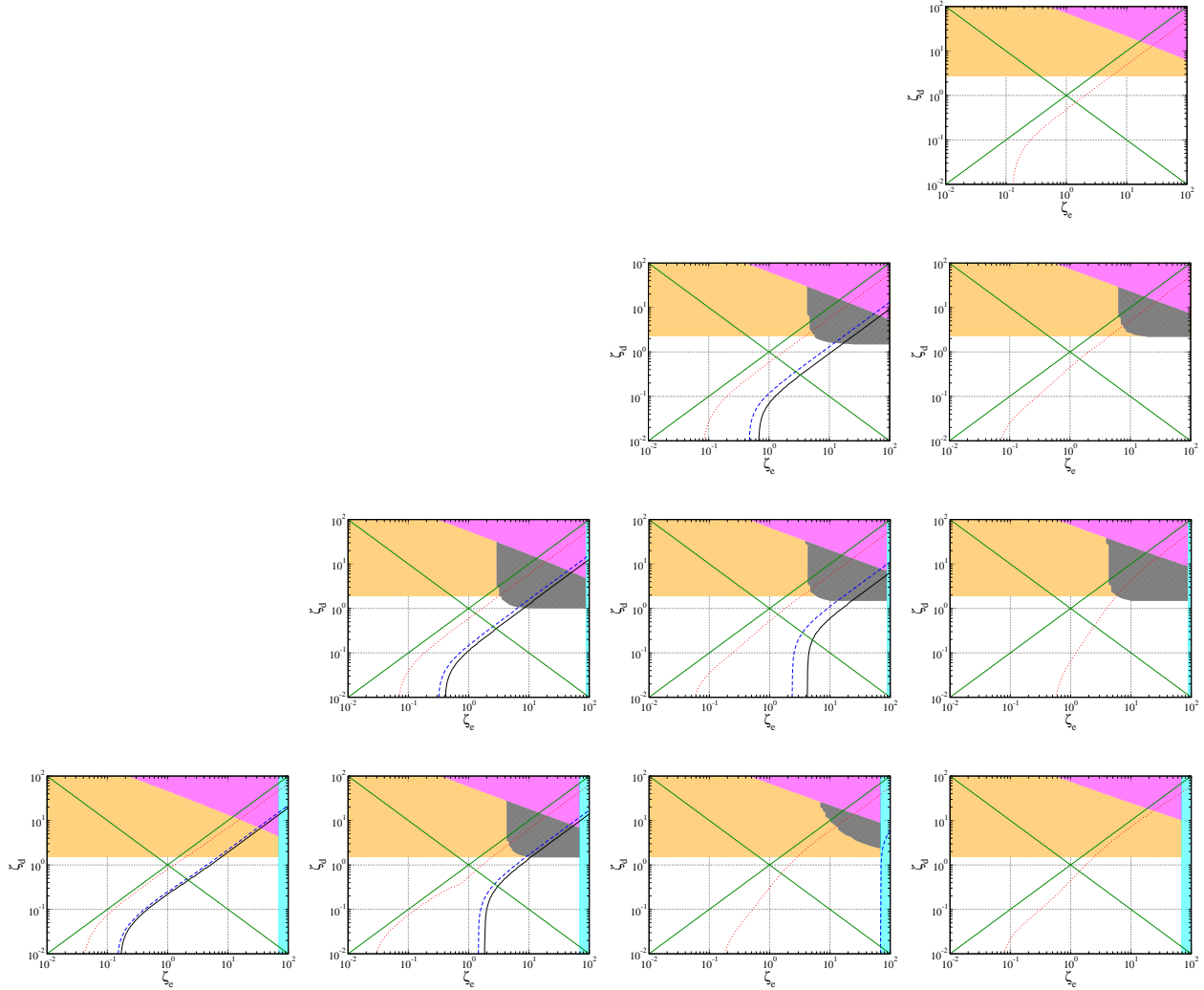


FIG. 6. Same as Fig. 5 but for the case with the light H^\pm scenario ($m_{H^\pm} = m_{H_2^0} \leq m_{H_3^0}$).

that in such a region the limit is slightly weaker. For $m_{H_2^0} = 280$ GeV with $|\Delta m| = 50$ GeV (right panel in the second row) and $m_{H_2^0} = 280$ GeV (top panel), no bound is obtained from the current LHC data, which is simply because of the smaller production cross section as compared with the case with $|\Delta m| = 0$. On the other hand, the HL-LHC sets the limit on ζ_e and ζ_d for these cases. The behavior of the flavor constraints is similar to that shown in Fig. 4, while the larger region can be excluded for the case with smaller m_{H^\pm} .

In Fig. 6, we see that the smaller area of the parameter region is excluded by the LHC data as compared with the heavy H^\pm scenario shown in Fig. 5. This is because H_3^0 can decay into not only $Z^{(*)}H_2^0$ but also $W^{\pm(*)}H^\pm$, where the former produces a tau lepton pair in its subsequent decay while the latter provides $\tau^\pm\nu$. In fact, it is seen that no bound is obtained for $|\Delta m| \geq 100$ GeV

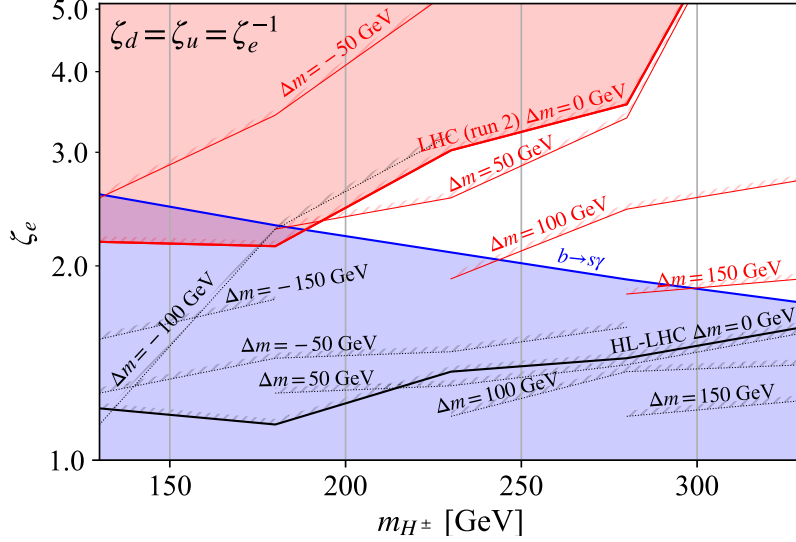


FIG. 7. Constraints on the parameter ζ_e in the Type-X THDM ($\zeta_u = \zeta_d = \zeta_e^{-1}$) as a function of the mass of H^\pm . The shaded regions are excluded by $B \rightarrow X_s \gamma$ (blue) and by the current LHC multi-lepton searches (red) with $\Delta m = 0$. The region above each red (black) curve is excluded by the multi-lepton searches at LHC (the HL-LHC) with several fixed value of Δm .

($|\Delta m| \geq 50$ GeV) for $m_{H_2^0} = 180$ and 230 GeV (280 GeV) from the current LHC data, while the HL-LHC can exclude a portion of the parameter space in such cases.

In Appendix A, we show the similar plots for $\zeta_u = 0$ in Figs. 9 and 10. The main difference in the collider study from the case with $\zeta_u = 0.1$ is the absence of $H_{2,3}^0 \rightarrow c\bar{c}$ and the $H^\pm \rightarrow tb$ decay being more suppressed. We can see that the above effects slightly make the LHC bound stronger particularly in the region with smaller ζ_e and ζ_d values as compared with the case with $\zeta_u = 0.1$. In addition, the constraint from $B \rightarrow X_s \gamma$ disappears in this case, so that the case with smaller ζ_e/ζ_d values is allowed.

Since the LHC bound is almost described by a line with a constant ζ_e/ζ_d value, we can extract the value of ζ_e along the line $\zeta_e = \zeta_d^{-1}$ as a representative point. In this way, we can set the upper limit on ζ_e as a function of the mass of the additional Higgs boson. We here particularly discuss the upper limit on ζ_e in the Type-X THDM which can be regarded as a special case of the aligned THDM, i.e., $\zeta_e = \zeta_d^{-1} = \zeta_u^{-1}$, see Eq. (10).

In Fig. 7, we show the constraints on the ζ_e value by the LHC multi-lepton searches as a function of m_{H^\pm} in the Type-X THDM ($\zeta_e = \zeta_d^{-1} = \zeta_u^{-1}$). The region above the red line is excluded, where the different lines correspond to the cases with different Δm . In particular, we fill

out the excluded region by a red color for $\Delta m = 0$. For the same m_{H^\pm} value, a larger Δm would set a stronger constraint. To see the difference between the heavy/light H^\pm scenarios discussed above, for example, comparing the sensitivity at $m_{H^\pm} = 200$ GeV for $\Delta m = 50$ GeV and that at $m_{H^\pm} = 250$ GeV for $\Delta m = -50$ GeV would be helpful, which share the same $m_{H_2^0}$ and $m_{H_3^0}$ values but with different m_{H^\pm} values. One can see the stronger constraint on ζ_e for the larger m_{H^\pm} case. In this figure, the blue shaded region describes the excluded region from the $B \rightarrow X_s \gamma$ data. One can see that most of the region is highly constrained for $\Delta m > 0$, and especially most of the parameter space is already excluded for $\Delta m = 150$ GeV when we restrict the masses of the additional Higgs bosons to be lighter than $2m_t$. The future HL-LHC reaches are shown by the black lines. There are almost no allowed region by combing the constraints from the HL-LHC and $B \rightarrow X_s \gamma$. Only exception is the case with $\Delta m = -100$ GeV, where the $H_3^0 \rightarrow H^\pm W^\mp$ and $H_3^0 \rightarrow H_2^0 Z$ modes dominate for such a small ζ_e case. The reason why the constraint on ζ_e for $\Delta m = -100$ GeV is weak compared with the case for $\Delta m = -150$ GeV at $m_{H^\pm} = 180$ GeV is that the $H_3^0 \rightarrow H_2^0 Z$ mode is relatively small compared with the $H_3^0 \rightarrow H^\pm W^\mp$ mode by the phase space suppression in the former case, where the $H_2^0 \rightarrow \tau^+ \tau^-$ mode provides an important contribution to the multi-lepton events. On the other hand, at $m_{H^\pm} = 130$ GeV, that for $\Delta m = -100$ GeV is strong compared with that for $\Delta m = -150$ GeV. This is because the $H_3^0 \rightarrow H^\pm W^\mp \rightarrow (\tau^+ \nu)(\tau^- \nu)$ mode provides an important contribution instead, where no competition between $\tau \nu$ and tb modes exists. We conclude that the Type-X THDM can be almost completely probed by the searches for the additional Higgs bosons at the HL-LHC when their masses are smaller than the $2m_t$. We note again that the constraints from $B \rightarrow X_s \gamma$ are sensitive to the complex phases of the ζ_f parameters.

D. Prospect for mass measurements of additional Higgs bosons

We consider here briefly the prospects of the mass measurements for the additional Higgs bosons at the HL-LHC. It is important as a basis of more dedicated study for the property measurements of additional Higgs bosons at LHC as well as the other future collider experiments including ILC. For example, the measurements of the CP property of the additional Higgs bosons at ILC has been discussed assuming the mass measurements are available at LHC [43]. We take the several benchmark points which are currently not excluded but in future possibly probed at LHC, and demonstrate the strategy to reconstruct the masses of the additional Higgs bosons. A summary of the benchmark points taken are shown in Table III.

We try to access the neutral Higgs boson masses using the $b\bar{b}\tau^+\tau^-$ mode, which is expected to

scenario	BPs	$m_{H_2^0}$	$m_{H_3^0}$	m_{H^\pm}
heavy H^\pm	BP1	280 GeV	180 GeV	280 GeV
	BP2	280 GeV	230 GeV	280 GeV
	BP3	230 GeV	180 GeV	230 GeV
light H^\pm	BP4	280 GeV	180 GeV	180 GeV

TABLE III. Summary of the benchmark points.

be the dominant decay mode in the available parameter region. It is because the region with too large ratio of ζ_e/ζ_d is already very constrained by the current LHC data as shown in the previous sections, which indicates that too large R_τ is not allowed unless the additional Higgs bosons are decoupled. As a selection cut we require a event should contain at least two b -tagged jets and at least two tau-tagged jets with $p_T > 20$ GeV, and $|\eta| < 2.5$. We also require $\cancel{E}_T > 50$ GeV. Since a visible hadronic tau jet carries only a part of the original tau lepton momentum due to the escaping neutrino momentum, we adopt the collinear approximation [96] to reconstruct the tau lepton momentum, assuming the transverse missing momentum $\cancel{\mathbf{p}}_T$ are generated solely by these neutrino momenta. The explicit procedure is to obtain c_1 and c_2 by solving the following relations,

$$\begin{aligned}
\mathbf{p}_{\tau_1} &= (1 + c_1)\mathbf{p}_{\tau_1}^{\text{vis}}, & \mathbf{p}_{\tau_2} &= (1 + c_2)\mathbf{p}_{\tau_2}^{\text{vis}} \quad (c_1, c_2 > 0), \\
\cancel{\mathbf{p}}_T &= c_1\mathbf{p}_{T,\tau_1}^{\text{vis}} + c_2\mathbf{p}_{T,\tau_2}^{\text{vis}}.
\end{aligned} \tag{38}$$

We only accept the events where the above equation has a solution. The larger the mass of the resonance is, the better this approximation provides the reconstructed tau momenta, since the momentum carried by the neutrino is aligned to the visible momentum. With the reconstructed tau momenta and bottom momenta we can compute $m_{\tau\tau}^{\text{rec}}$ and m_{bb} each event. In Fig. 8, the 2-dimensional m_{bb} vs. $m_{\tau\tau}$ distributions are shown as a scattering plot in the left panels for BP1 to BP4 from top to bottom. The dense regions are depicted in red points. In all cases, dense regions are observed either at the corresponding $(m_{H_2^0}, m_{H_3^0})$, $(m_{H_3^0}, m_{H_2^0})$, and $(m_{H_2^0}, m_{H_2^0})$ in each BP.

The central and right panels show the corresponding $\min(m_{bb}, m_{\tau\tau}^{\text{rec}})$ and $\max(m_{bb}, m_{\tau\tau}^{\text{rec}})$ projected distributions, respectively. The expected number of events for 3 ab^{-1} at HL-LHC including the effects of the selection cut and the efficiencies are shown in the plots. The total and the breakdown of the contributions from the six production modes are plotted. One can see that the $\min(m_{bb}, m_{\tau\tau}^{\text{rec}})$ distribution exhibits the peak at the corresponding $m_{H_2^0}$ and the $\max(m_{bb}, m_{\tau\tau}^{\text{rec}})$ distribution does at the $m_{H_3^0}$ in each BP. For the benchmark points in the heavy H^\pm scenarios (BP1, BP2, BP3), all production modes contribute to the peak at $m_{H_2^0}$ in the $\min(m_{bb}, m_{\tau\tau})$

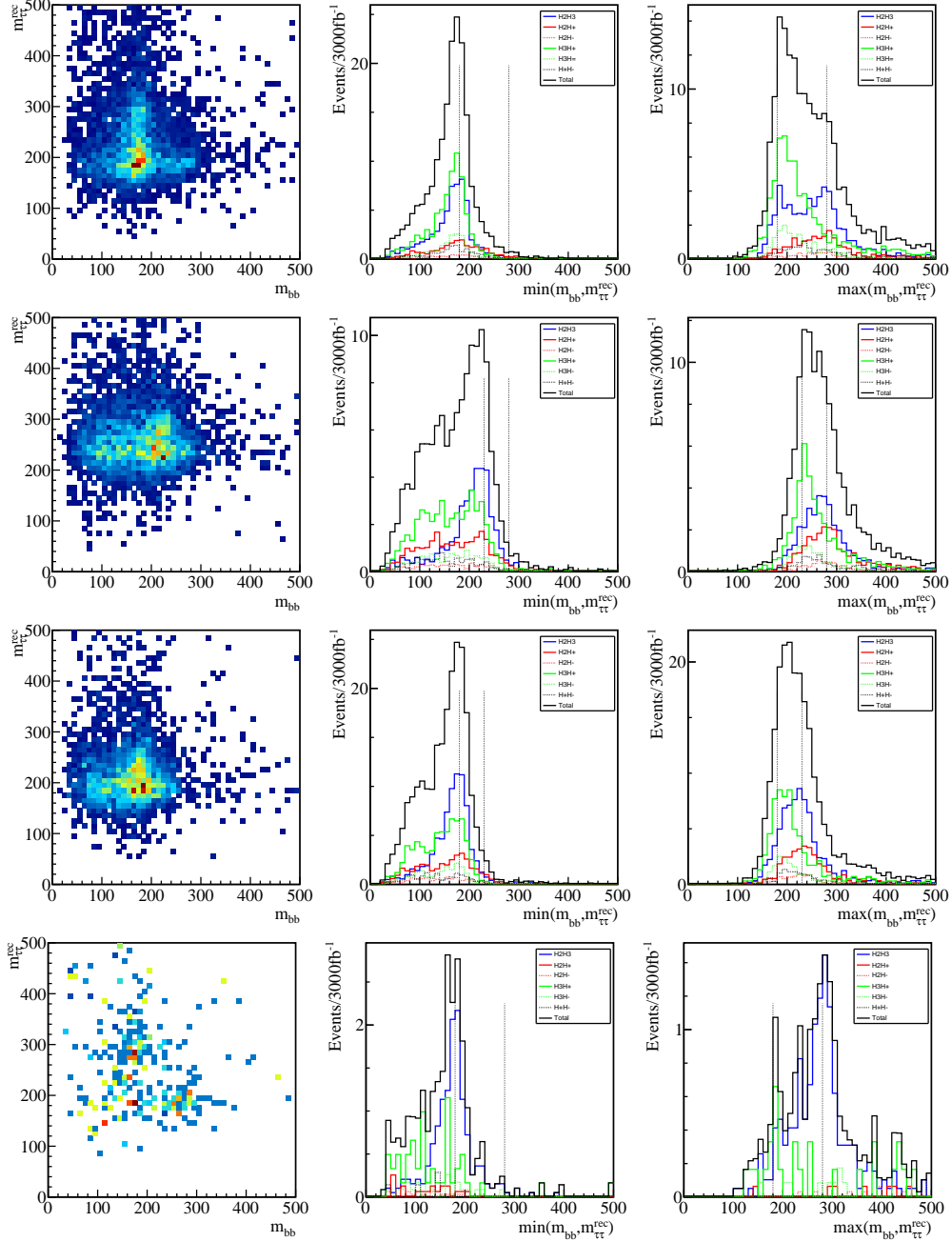


FIG. 8. 2-dimensional m_{bb} vs. $m_{\tau\tau}^{\text{rec}}$ distributions (left panels), $\min(m_{bb}, m_{\tau\tau}^{\text{rec}})$ distributions (central panels), and $\max(m_{bb}, m_{\tau\tau}^{\text{rec}})$ distributions (right panels) in the $2b2\tau$ events at BP1 - BP4 from top to bottom.

distributions. In the $\max(m_{bb}, m_{\tau\tau}^{\text{rec}})$ distributions only the H_2H_3 and H_2H^\pm production modes contribute to the peak at $m_{H_3^0}$ as expected, while all modes contribute to the peak at $m_{H_2^0}$. The corresponding $m_{H_2^0}$ and $m_{H_3^0}$ values are indicated by the vertical dashed lines in each plot.

For the light H^\pm scenario (BP4), only the H_2H_3 production mode essentially contributes to these distributions since the decays involving charged Higgs bosons do not produce events to fulfill the $2b2\tau$ selection criteria. Therefore, the expected number of the signals is much smaller than the

cases in the heavy H^\pm scenario, although the BP4 has the lightest mass spectrum and the total production cross section is the largest among those of the four benchmark points. Accessing the charged Higgs mass would be also possible, for example, following a similar procedure proposed in Ref. [97], although we leave it for a future study.

As we have seen in this section, the masses of the additional Higgs bosons can be in principle determined using these characteristic peaks in the proposed distributions in the mass range we consider, whereas it would be rather difficult when the charged Higgs boson is the lightest among the three additional Higgs bosons. For quantitative estimation of the precision of the mass measurements, clearly more dedicated signal and background analyses are necessary for our benchmark scenarios, as performed in the different occasion in Ref. [59]. It is beyond the scope of this paper, but we plan to do it as a future work.

VI. CONCLUSIONS AND DISCUSSIONS

We have discussed the double-aligned THDM, where the coupling constants of the discovered Higgs boson to the SM particles are identical to those of the SM Higgs boson, and the FCNCs do not appear at tree level. This scenario is well motivated by the scenario of EW baryogenesis, which is compatible with the current experimental data. In the double-aligned scenario, the additional Higgs bosons can mainly decay into a fermion pair or a lighter Higgs boson associated with a gauge boson depending on the ζ_f parameters and the masses of the additional Higgs bosons. We have discussed the behavior of the branching ratios in details especially for the CP conserving case. We then have explicitly shown the critical values of the ζ_f parameters, at which the sum of the branching ratios to the fermion pairs is 50%. In addition, we have investigated the current constraints on the parameter space from the various flavor experiments, i.e., $B \rightarrow X_s \gamma$, $B_s \rightarrow \mu\mu$ and the tau decay, and from the searches in the multi-lepton final states at the LHC Run-II experiment. For the collider constraints, we particularly focused on the EW pair production of the additional Higgs bosons with their masses below $2m_t$, whose production cross sections are simply determined by the masses of the Higgs bosons. It has been found that a large portion of the parameter space is already excluded by the current LHC data when the leptonic decays of the additional Higgs bosons are dominant. As a result, we have found that the remaining parameter space should satisfy $|\zeta_d/\zeta_e| \gtrsim \mathcal{O}(1)$. Our results can be interpreted to the scenario in the Type-X THDM as a special case. In the case where all the additional Higgs bosons are degenerate in mass, we have found that the mass below 190 GeV has been already excluded by the data from the LHC

Run-II in the Type-X THDM. If there is the mass difference the constraint is stronger. Namely, the charged Higgs mass below 250 GeV (300 GeV) has been excluded for $\Delta m = 100$ GeV (150 GeV). Furthermore, at the HL-LHC we have shown that most of the parameter region in the Type-X THDM would be explored. Since the available parameter region tends to predict a significant amount of the $b\bar{b}$ branching ratios for the additional Higgs bosons, we have demonstrated the reconstruction of the masses of additional Higgs bosons from the $b\bar{b}\tau^+\tau^-$ final state in a few benchmark points. Extension to the analysis with CP violating phases will be performed elsewhere.

ACKNOWLEDGMENTS

This work was supported, in part, by the Grant-in-Aid on Innovative Areas, the Ministry of Education, Culture, Sports, Science and Technology, No. 16H06492, and by the JSPS KAKENHI Grant No. 20H00160 [SK, MT], the Grant-in-Aid for Scientific Research C, No. 18K03611 [MT] and the Grant-in-Aid for Early-Career Scientists, No. 19K14714 [KY].

Appendix A: The results for $\zeta_u = 0$

In this appendix, we show the plots as Fig. 5 and Fig. 6 in the heavy charged Higgs scenario and in the light charged Higgs scenario for $\zeta_u = 0$. Due to the suppression of the $H_{2,3} \rightarrow c\bar{c}$ and $H^\pm \rightarrow tb$ decay modes, stronger constraints are in general obtained from the LHC multi-lepton searches.

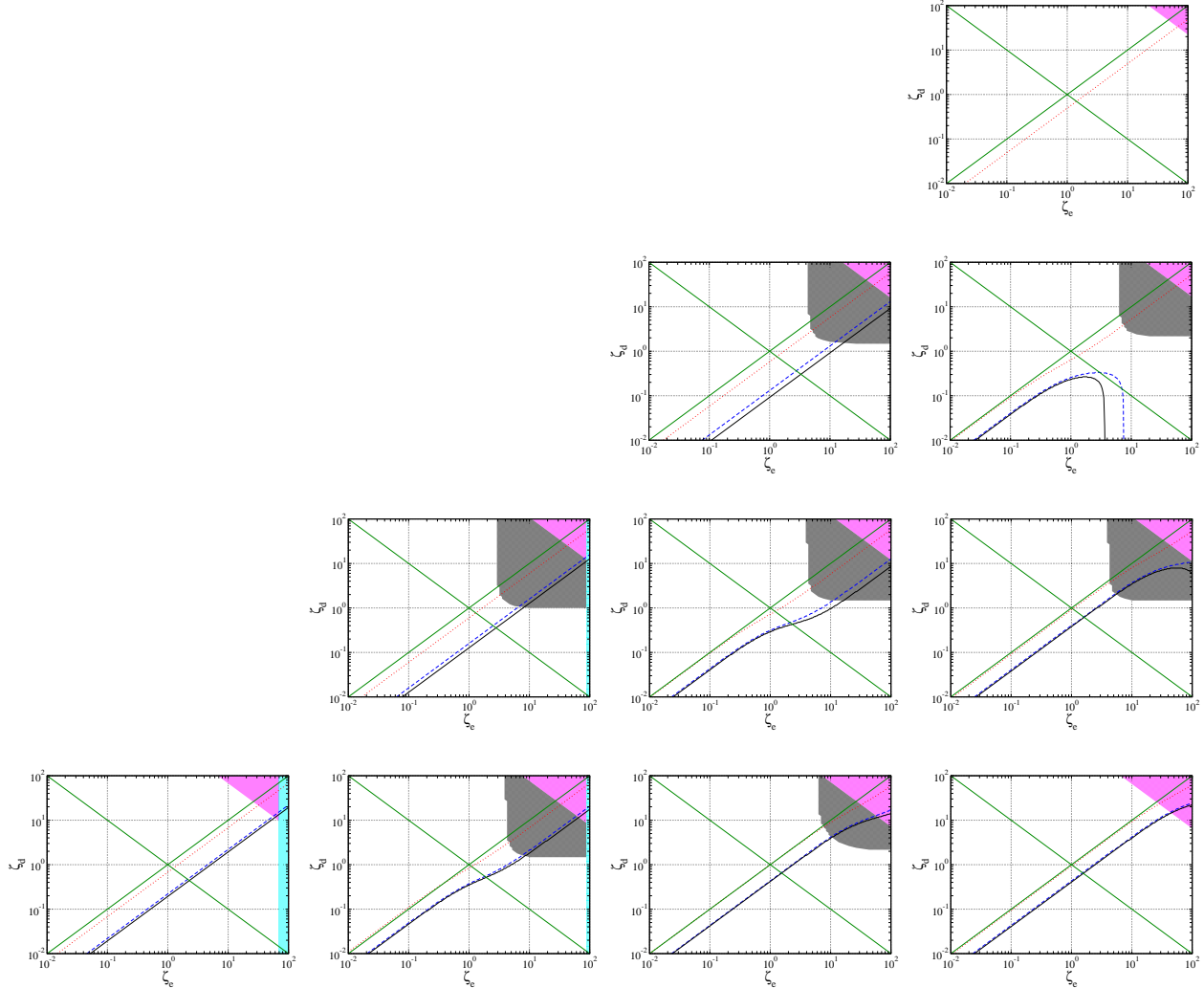


FIG. 9. The same plots as Fig. 5 but for $\zeta_u = 0$ in the heavy H^\pm scenario ($m_{H_2^0} \leq m_{H_3^0} = m_{H^\pm}$).

-
- [1] H. E. Haber and G. L. Kane, Phys. Rept. **117**, 75 (1985).
 - [2] E. Ma, Phys. Rev. Lett. **86**, 2502 (2001), arXiv:hep-ph/0011121.
 - [3] A. Zee, Phys. Lett. **93B**, 389 (1980), [Erratum: Phys. Lett.95B,461(1980)].

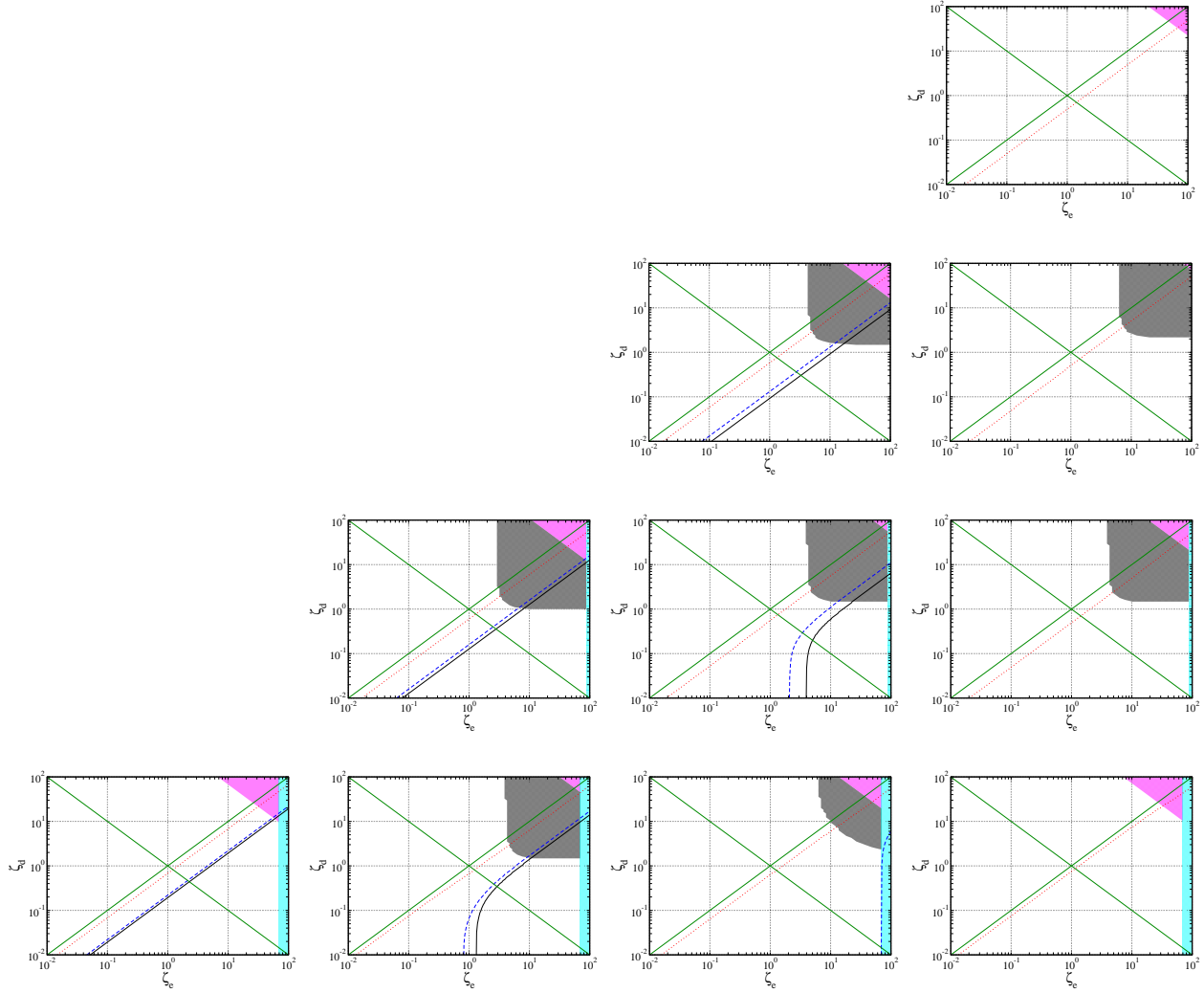


FIG. 10. The same plots as Fig. 6 but for $\zeta_u = 0$ in the light H^\pm scenario ($m_{H_2^\pm} = m_{H^\pm} \leq m_{H_3^0}$).

- [4] E. Ma, Phys. Rev. D **73**, 077301 (2006), arXiv:hep-ph/0601225.
- [5] M. Aoki, S. Kanemura, and O. Seto, Phys. Rev. Lett. **102**, 051805 (2009), arXiv:0807.0361 [hep-ph].
- [6] R. Barbieri, L. J. Hall, and V. S. Rychkov, Phys. Rev. D **74**, 015007 (2006), arXiv:hep-ph/0603188.
- [7] S. Kanemura, Y. Okada, and E. Senaha, Phys. Lett. B **606**, 361 (2005), arXiv:hep-ph/0411354.
- [8] L. Fromme, S. J. Huber, and M. Seniuch, JHEP **11**, 038 (2006), arXiv:hep-ph/0605242.
- [9] K. Funakubo, A. Kakuto, and K. Takenaga, Prog. Theor. Phys. **91**, 341 (1994), arXiv:hep-ph/9310267.
- [10] N. Turok and J. Zadrozny, Nucl. Phys. B **358**, 471 (1991).
- [11] J. M. Cline, K. Kainulainen, and A. P. Vischer, Phys. Rev. D **54**, 2451 (1996), arXiv:hep-ph/9506284.
- [12] T. Modak and E. Senaha, Phys. Rev. D **99**, 115022 (2019), arXiv:1811.08088 [hep-ph].
- [13] P. Basler, M. Mühlleitner, and J. Müller, (2021), arXiv:2108.03580 [hep-ph].
- [14] S. L. Glashow and S. Weinberg, Phys. Rev. D **15**, 1958 (1977).
- [15] Y. Grossman, Nucl. Phys. **B426**, 355 (1994), arXiv:hep-ph/9401311 [hep-ph].

- [16] M. Aoki, S. Kanemura, K. Tsumura, and K. Yagyu, Phys. Rev. **D80**, 015017 (2009), arXiv:0902.4665 [hep-ph].
- [17] V. D. Barger, J. L. Hewett, and R. J. N. Phillips, Phys. Rev. **D41**, 3421 (1990).
- [18] A. Pich and P. Tuzon, Phys. Rev. D **80**, 091702 (2009), arXiv:0908.1554 [hep-ph].
- [19] T. Appelquist and J. Carazzone, Phys. Rev. D **11**, 2856 (1975).
- [20] J. F. Gunion and H. E. Haber, Phys. Rev. D **67**, 075019 (2003), arXiv:hep-ph/0207010.
- [21] S. Davidson and H. E. Haber, Phys. Rev. D **72**, 035004 (2005), [Erratum: Phys.Rev.D 72, 099902 (2005)], arXiv:hep-ph/0504050.
- [22] M. Aiko, S. Kanemura, M. Kikuchi, K. Mawatari, K. Sakurai, and K. Yagyu, Nucl. Phys. B **966**, 115375 (2021), arXiv:2010.15057 [hep-ph].
- [23] S. Kanemura, Y. Okada, E. Senaha, and C. P. Yuan, Phys. Rev. D **70**, 115002 (2004), arXiv:hep-ph/0408364.
- [24] S. Kanemura, M. Kikuchi, and K. Yagyu, Nucl. Phys. B **896**, 80 (2015), arXiv:1502.07716 [hep-ph].
- [25] S. Kanemura and R. Nagai, (2021), arXiv:2111.12585 [hep-ph].
- [26] J. Braathen and S. Kanemura, Phys. Lett. B **796**, 38 (2019), arXiv:1903.05417 [hep-ph].
- [27] J. Braathen and S. Kanemura, Eur. Phys. J. C **80**, 227 (2020), arXiv:1911.11507 [hep-ph].
- [28] T. Plehn, M. Spira, and P. M. Zerwas, Nucl. Phys. B **479**, 46 (1996), [Erratum: Nucl.Phys.B 531, 655–655 (1998)], arXiv:hep-ph/9603205.
- [29] U. Baur, T. Plehn, and D. L. Rainwater, Phys. Rev. Lett. **89**, 151801 (2002), arXiv:hep-ph/0206024.
- [30] U. Baur, T. Plehn, and D. L. Rainwater, Phys. Rev. D **67**, 033003 (2003), arXiv:hep-ph/0211224.
- [31] E. Asakawa, D. Harada, S. Kanemura, Y. Okada, and K. Tsumura, Phys. Rev. D **82**, 115002 (2010), arXiv:1009.4670 [hep-ph].
- [32] A. J. Barr, M. J. Dolan, C. Englert, D. E. Ferreira de Lima, and M. Spannowsky, JHEP **02**, 016 (2015), arXiv:1412.7154 [hep-ph].
- [33] A. Papaefstathiou, Phys. Rev. D **91**, 113016 (2015), arXiv:1504.04621 [hep-ph].
- [34] Q.-H. Cao, G. Li, B. Yan, D.-M. Zhang, and H. Zhang, Phys. Rev. D **96**, 095031 (2017), arXiv:1611.09336 [hep-ph].
- [35] D. Gonçalves, T. Han, F. Kling, T. Plehn, and M. Takeuchi, Phys. Rev. D **97**, 113004 (2018), arXiv:1802.04319 [hep-ph].
- [36] A. Biekötter, D. Gonçalves, T. Plehn, M. Takeuchi, and D. Zerwas, SciPost Phys. **6**, 024 (2019), arXiv:1811.08401 [hep-ph].
- [37] A. Abada *et al.* (FCC), Eur. Phys. J. C **79**, 474 (2019).
- [38] A. Abada *et al.* (FCC), Eur. Phys. J. ST **228**, 1109 (2019).
- [39] H. Aihara *et al.* (ILC), (2019), arXiv:1901.09829 [hep-ex].
- [40] J. Klamka (CLICdp), in *European Physical Society Conference on High Energy Physics 2021* (2021) arXiv:2111.04787 [hep-ex].
- [41] T. Han, D. Liu, I. Low, and X. Wang, Phys. Rev. D **103**, 013002 (2021), arXiv:2008.12204 [hep-ph].

- [42] M. Chiesa, F. Maltoni, L. Mantani, B. Mele, F. Piccinini, and X. Zhao, *JHEP* **09**, 098 (2020), arXiv:2003.13628 [hep-ph].
- [43] S. Kanemura, M. Kubota, and K. Yagyu, *JHEP* **08**, 026 (2020), arXiv:2004.03943 [hep-ph].
- [44] V. Andreev *et al.* (ACME), *Nature* **562**, 355 (2018).
- [45] C. Abel *et al.* (nEDM), *Phys. Rev. Lett.* **124**, 081803 (2020), arXiv:2001.11966 [hep-ex].
- [46] K. Cheung, A. Jueid, Y.-N. Mao, and S. Moretti, *Phys. Rev. D* **102**, 075029 (2020), arXiv:2003.04178 [hep-ph].
- [47] T. Abe, J. Hisano, T. Kitahara, and K. Tobioka, *JHEP* **01**, 106 (2014), [Erratum: *JHEP* **04**, 161 (2016)], arXiv:1311.4704 [hep-ph].
- [48] M. Jung and A. Pich, *JHEP* **04**, 076 (2014), arXiv:1308.6283 [hep-ph].
- [49] W. Altmannshofer, S. Gori, N. Hamer, and H. H. Patel, *Phys. Rev. D* **102**, 115042 (2020), arXiv:2009.01258 [hep-ph].
- [50] I. Low, N. R. Shah, and X.-P. Wang, (2020), arXiv:2012.00773 [hep-ph].
- [51] K. Enomoto, S. Kanemura, and Y. Mura, (2021), arXiv:2111.13079 [hep-ph].
- [52] S. Kanemura, M. Kubota, and K. Yagyu, *JHEP* **04**, 144 (2021), arXiv:2101.03702 [hep-ph].
- [53] H. Baer, T. Barklow, K. Fujii, Y. Gao, A. Hoang, S. Kanemura, J. List, H. E. Logan, A. Nomerotski, M. Perelstein, *et al.*, (2013), arXiv:1306.6352 [hep-ph].
- [54] S. Asai, J. Tanaka, Y. Ushiroda, M. Nakao, J. Tian, S. Kanemura, S. Matsumoto, S. Shirai, M. Endo, and M. Kakizaki, (2017), arXiv:1710.08639 [hep-ex].
- [55] K. Fujii *et al.*, (2017), arXiv:1710.07621 [hep-ex].
- [56] C.-S. S. Group, (2015).
- [57] M. Bicer *et al.* (TLEP Design Study Working Group), *Proceedings, 2013 Community Summer Study on the Future of U.S. Particle Physics: Snowmass on the Mississippi (CSS2013): Minneapolis, MN, USA, July 29-August 6, 2013*, *JHEP* **01**, 164 (2014), arXiv:1308.6176 [hep-ex].
- [58] S. Kanemura and C. P. Yuan, *Phys. Lett. B* **530**, 188 (2002), arXiv:hep-ph/0112165.
- [59] Q.-H. Cao, S. Kanemura, and C. P. Yuan, *Phys. Rev. D* **69**, 075008 (2004), arXiv:hep-ph/0311083.
- [60] A. Belyaev, Q.-H. Cao, D. Nomura, K. Tobe, and C. P. Yuan, *Phys. Rev. Lett.* **100**, 061801 (2008), arXiv:hep-ph/0609079.
- [61] O. Eberhardt, A. P. n. Martínez, and A. Pich, *JHEP* **05**, 005 (2021), arXiv:2012.09200 [hep-ph].
- [62] S. M. Barr and A. Zee, *Phys. Rev. Lett.* **65**, 21 (1990), [Erratum: *Phys.Rev.Lett.* **65**, 2920 (1990)].
- [63] M. E. Peskin and T. Takeuchi, *Phys. Rev. Lett.* **65**, 964 (1990).
- [64] S. Bertolini, *Nucl. Phys.* **B272**, 77 (1986).
- [65] M. E. Peskin and J. D. Wells, *Phys. Rev.* **D64**, 093003 (2001), arXiv:hep-ph/0101342 [hep-ph].
- [66] W. Grimus, L. Lavoura, O. M. Ogreid, and P. Osland, *Nucl. Phys.* **B801**, 81 (2008), arXiv:0802.4353 [hep-ph].
- [67] S. Kanemura, Y. Okada, H. Taniguchi, and K. Tsumura, *Phys. Lett.* **B704**, 303 (2011), arXiv:1108.3297 [hep-ph].

- [68] M. Aoki, S. Kanemura, and K. Yagyu, *Phys. Rev. D* **85**, 055007 (2012), arXiv:1110.4625 [hep-ph].
- [69] M. Capdequi Peyranere, H. E. Haber, and P. Irulegui, *Phys. Rev. D* **44**, 191 (1991).
- [70] S. Kanemura, *Phys. Rev. D* **61**, 095001 (2000), arXiv:hep-ph/9710237.
- [71] P. A. Zyla *et al.* (Particle Data Group), *PTEP* **2020**, 083C01 (2020).
- [72] A. Alberti, P. Gambino, K. J. Healey, and S. Nandi, *Phys. Rev. Lett.* **114**, 061802 (2015), arXiv:1411.6560 [hep-ph].
- [73] S. Aoki *et al.* (Flavour Lattice Averaging Group), *Eur. Phys. J. C* **80**, 113 (2020), arXiv:1902.08191 [hep-lat].
- [74] Y. S. Amhis *et al.* (HFLAV), *Eur. Phys. J. C* **81**, 226 (2021), arXiv:1909.12524 [hep-ex].
- [75] J. Charles *et al.*, *Phys. Rev. D* **91**, 073007 (2015), arXiv:1501.05013 [hep-ph].
- [76] M. Czakon, P. Fiedler, T. Huber, M. Misiak, T. Schutzmeier, and M. Steinhauser, *JHEP* **04**, 168 (2015), arXiv:1503.01791 [hep-ph].
- [77] M. Ciuchini, G. Degrossi, P. Gambino, and G. F. Giudice, *Nucl. Phys. B* **527**, 21 (1998), arXiv:hep-ph/9710335.
- [78] M. Misiak and M. Steinhauser, *Eur. Phys. J. C* **77**, 201 (2017), arXiv:1702.04571 [hep-ph].
- [79] F. Borzumati and C. Greub, *Phys. Rev. D* **58**, 074004 (1998), arXiv:hep-ph/9802391.
- [80] A. L. Kagan and M. Neubert, *Eur. Phys. J. C* **7**, 5 (1999), arXiv:hep-ph/9805303.
- [81] X.-Q. Li, J. Lu, and A. Pich, *JHEP* **06**, 022 (2014), arXiv:1404.5865 [hep-ph].
- [82] C. Bobeth, M. Gorbahn, T. Hermann, M. Misiak, E. Stamou, and M. Steinhauser, *Phys. Rev. Lett.* **112**, 101801 (2014), arXiv:1311.0903 [hep-ph].
- [83] M. Krawczyk and D. Temes, *Eur. Phys. J. C* **44**, 435 (2005), arXiv:hep-ph/0410248.
- [84] J. R. Ellis, M. K. Gaillard, and D. V. Nanopoulos, *Nucl. Phys. B* **106**, 292 (1976).
- [85] E. Eichten, I. Hinchliffe, K. D. Lane, and C. Quigg, *Rev. Mod. Phys.* **56**, 579 (1984), [Addendum: *Rev.Mod.Phys.* **58**, 1065–1073 (1986)].
- [86] J. F. Gunion and H. E. Haber, *Nucl. Phys. B* **278**, 449 (1986), [Erratum: *Nucl.Phys.B* **402**, 569–569 (1993)].
- [87] A. Djouadi, W. Kilian, M. Muhlleitner, and P. M. Zerwas, *Eur. Phys. J. C* **10**, 45 (1999), arXiv:hep-ph/9904287.
- [88] S. Kanemura, K. Tsumura, and H. Yokoya, *Phys. Rev. D* **85**, 095001 (2012), arXiv:1111.6089 [hep-ph].
- [89] E. J. Chun, Z. Kang, M. Takeuchi, and Y.-L. S. Tsai, *JHEP* **11**, 099 (2015), arXiv:1507.08067 [hep-ph].
- [90] G. Aad *et al.* (ATLAS), (2021), 10.1007/JHEP07(2021)167, arXiv:2103.11684 [hep-ex].
- [91] A. Tumasyan *et al.* (CMS), (2021), arXiv:2106.14246 [hep-ex].
- [92] J. Alwall, M. Herquet, F. Maltoni, O. Mattelaer, and T. Stelzer, *JHEP* **06**, 128 (2011), arXiv:1106.0522 [hep-ph].
- [93] T. Sjostrand, S. Mrenna, and P. Z. Skands, *Comput. Phys. Commun.* **178**, 852 (2008), arXiv:0710.3820 [hep-ph].

- [94] J. de Favereau, C. Delaere, P. Demin, A. Giammanco, V. Lemaître, A. Mertens, and M. Selvaggi (DELPHES 3), *JHEP* **02**, 057 (2014), arXiv:1307.6346 [hep-ex].
- [95] G. Aad *et al.* (ATLAS), *Phys. Rev. Lett.* **125**, 051801 (2020), arXiv:2002.12223 [hep-ex].
- [96] D. L. Rainwater, D. Zeppenfeld, and K. Hagiwara, *Phys. Rev. D* **59**, 014037 (1998), arXiv:hep-ph/9808468.
- [97] S. Iguro, Y. Omura, and M. Takeuchi, *JHEP* **11**, 130 (2019), arXiv:1907.09845 [hep-ph].